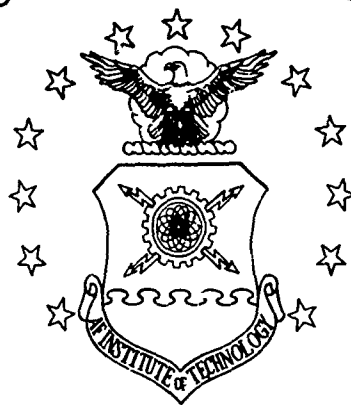
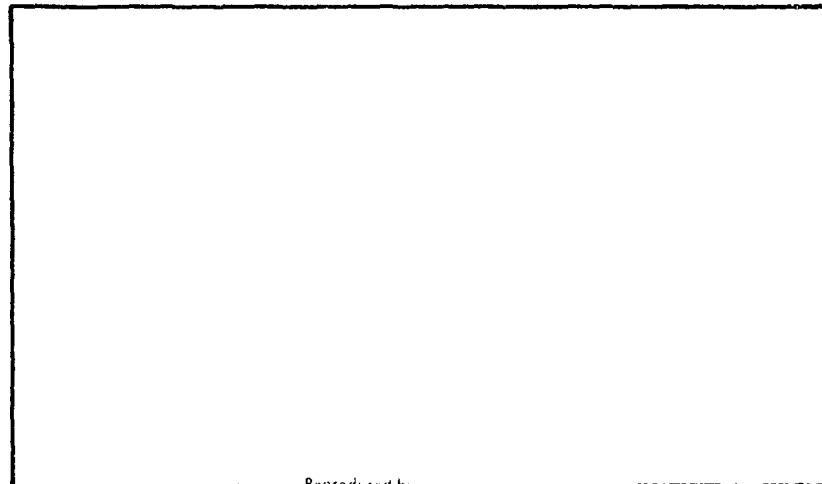


AD753387

AIR FORCE INSTITUTE OF TECHNOLOGY



AIR UNIVERSITY  
UNITED STATES AIR FORCE



Reproduced by  
NATIONAL TECHNICAL  
INFORMATION SERVICE  
U.S. Department of Commerce  
Springfield, VA 22151

SCHOOL OF ENGINEERING

WRIGHT-PATTERSON AIR FORCE BASE, OHIO

DDC  
RECEIVED  
2 1973  
RESERVED

Unclassified

Security Classification

DOCUMENT CONTROL DATA - R & D

(Security classification of title, body of abstract and indexing annotation must be entered when the overall report is classified)

1. ORIGINATING ACTIVITY (Corporate author) <b>Air Force Institute of Technology Wright-Patterson Air Force Base, Ohio 45433</b>	2a. REPORT SECURITY CLASSIFICATION <b>Unclassified</b> 2b. GROUP
--	--

3. REPORT TITLE  
**AN ANALYSIS OF THE FLOW FIELD AROUND A 2-D BODY OF ARBITRARY SHAPE**

4. DESCRIPTIVE NOTES (Type of report and inclusive dates)  
**AFIT Thesis**

5. AUTHOR(S) (First name, middle initial, last name)  
**Ellie B. Underwood, Jr.  
Capt USAF**

6. REPORT DATE <b>December 1971</b>	7a. TOTAL NO. OF PAGES <b>27 87</b>	7b. NO. OF REFS <b>4</b>
--	--	-----------------------------

8a. CONTRACT OR GRANT NO.  b. PROJECT NO. <b>N/A</b>  c.  d.	9a. ORIGINATOR'S REPORT NUMBER(S) <b>GAM-AE/72-2</b>  9b. OTHER REPORT NO(S) (Any other numbers that may be assigned this report)
--	--

10. DISTRIBUTION STATEMENT  
**Approved for public release; distribution unlimited.**

Approved for public release; IAW AFR 190-217 <b>JERRY C. HIX, Captain, USAF Director of Information</b>	11. SPONSORING MILITARY ACTIVITY <b>AFIT-EN</b>
--	--

13. ABSTRACT  
An analytical study of the two-dimensional viscous, incompressible steady flow over an airfoil of arbitrary shape was made. Theodorsen's method was used to analyze the potential flow around the airfoil, providing edge velocities for the boundary layer equations, which were then solved by the Karman-Pohlhausen method. The resulting boundary layer displacement thickness was then added to the original airfoil shape to obtain a better potential flow solution. Iteration was continued in this manner until the desired accuracy was obtained. A computer program was written to effect this airfoil analysis technique. Potential flow surface velocity distribution, angle of attack at zero lift, and wall shearing stress were shown to agree well with results of other investigators.

- 1a -

14.

KEY WORDS

LINK A

LINK B

LINK C

ROLE

WT

ROLE

WT

ROLE

WT

Airfoil

Theodorsen

Conformal transformation

Potential flow

Boundary layer

AN ANALYSIS OF THE FLOW FIELD AROUND A 2-D  
BODY OF ARBITRARY SHAPE

THESIS

Presented to the Faculty of the School of Engineering  
of the Air Force Institute of Technology  
Air University  
in Partial Fulfillment of the  
Requirements for the Degree of  
Master of Science

by

Ellie B. Underwood, Jr., B.S.A.S.E.  
Captain USAF  
Graduate Aeronautical Engineering

December 1971

-ic-

Approved for public release; distribution unlimited.

Contents

List of Figures . . . . .	iii
List of Tables . . . . .	iv
List of Symbols . . . . .	v
Abstract . . . . .	viii
I. Introduction . . . . .	1
II. Theodorsen's Method . . . . .	6
III. Karman-Pohlhausen Method . . . . .	21
IV. Computer Study . . . . .	33
V. Results . . . . .	36
VI. Conclusions and Recommendations . . . . .	43
Bibliography . . . . .	45
Appendix A: Computer Program and Sample Output Format . . . . .	46
Vita . . . . .	

List of Figures

<u>Figure</u>		<u>Page</u>
1	Transformation Planes and Notation . . . . .	10
2	Boundary Layer Coordinate System . . . . .	22
3	Transformation of NACA 4424 Airfoil . . . . .	38
4	Pressure Distribution on NACA 1408 Airfoil . . . . .	39
5	Shear Stress on NACA 1408 Airfoil . . . . .	40
6	Boundary Layer Displacement Thickness on NACA 1408 Airfoil . . . . .	41

List of Tables

<u>Table</u>		<u>Page</u>
1	Comparison of Zero Lift Angles of Attack . . . . .	36
2	Comparison of Potential Flow Velocities for NACA 1408 Airfoil . . . . .	37

List of SymbolsFor Theodorsen's Method

<u>Symbol</u>	<u>Description</u>
a	Dimensional proportionality constant (length)
$A_n, B_n, C_n$	Fourier coefficients
i	$\sqrt{-1}$
m	Intermediate quantity in Joukowski transformation, defined on page 9
R	Radius vector in exact circle plane
u	Velocity in x-direction
V	Potential flow surface velocity
$V_\infty$	Freestream velocity
v	Velocity in y-direction
w	Complex potential function
x	Cartesian coordinate in freestream flow direction
y	Cartesian coordinate perpendicular to freestream flow direction
z	Complex position vector in exact circle plane
$z'$	Complex position vector in pseudo-circle plane
$\alpha$	Angle of attack
$\beta$	Angle of attack at zero lift
$\Gamma$	Circulation
$\epsilon$	Conformal angular distortion function
$\zeta$	Complex position vector in airfoil plane
$\theta$	Angular measure in exact circle plane
$\lambda$	Dummy variable of integration corresponding to $\theta$

<u>Symbol</u>	<u>Description</u>
$\rho$	Radius vector in pseudo-circle plane
$\phi$	Potential function
$\phi$	Magnification exponent in exact circle plane
$\Psi$	Stream function
$\psi$	Magnification exponent in pseudo-circle plane, as a function of $\omega$
$\bar{\psi}$	$\psi$ , as a function of $\theta$
$\omega$	Angular measure in pseudo-circle plane

For Karman-Pohlhausen Method

<u>Symbol</u>	<u>Description</u>
a,b,c,d	Coefficients in assumed velocity profile
F,f <sub>1</sub> ,f <sub>2</sub> ,Z,K	Boundary layer parameters
U	Boundary layer edge velocity
x	Streamwise coordinate
y	Cross-stream coordinate
$\delta$	Boundary layer thickness
$\delta_1$	Boundary layer displacement thickness
$\delta_2$	Boundary layer momentum thickness
$\eta$	Cross-stream coordinate referenced to boundary layer thickness, $y/\delta$
$\Lambda$	Shape factor
$\mu$	Absolute viscosity
$\nu$	Dynamic viscosity
$\rho$	Fluid density
$\tau_w$	Shear stress at airfoil surface
o	Subscript indicating stagnation point

Symbol

Description

1

Subscript indicating first point downstream  
of stagnation point

n

Subscript indicating general point

AN ANALYSIS OF THE FLOW FIELD AROUND A 2-D  
BODY OF ARBITRARY SHAPE

I. Introduction

Purpose

The purpose of this study was to determine the velocity field and, therefore, the pressure distribution about a body of arbitrary shape in a two-dimensional, steady, incompressible, constant viscosity flow, utilizing a combination of Theodorsen's method and the Karman-Pohlhausen method. A computer program to implement this combined method has been written, and results from this program are described herein.

Some practical and theoretical considerations leading to this combined method are presented in the remainder of this section.

Background

The theoretical analysis or design of an airfoil shape is based primarily upon a knowledge of the velocity field in the neighborhood of the body. Since the time of Prandtl, aerodynamicists have realized that the flow over a body could be divided, for purposes of analysis, into two regions. Observations indicate that viscous forces predominate over inertia forces in a very thin layer near the surface of the body, and this region has come to be called the boundary layer. Outside this region, the flow may, with little error, be considered inviscid. Since inviscid flow with a

uniform parallel onset velocity may be described in terms of a velocity potential, the inviscid region is also called the region of potential flow. If the velocity field can be determined in the inviscid flow, then the velocity at the edge of the boundary layer will be known and may be used as a boundary condition for solution of the boundary layer equations. Each of these regions will now be considered.

#### Region of Inviscid Flow

For thin streamlined airfoils at low angles of attack, small perturbation theory permits a number of simplifying assumptions in the equations of motion for inviscid flow. However, no such simplified potential theory was available for airfoils of arbitrary shape until 1933, when Theodorsen's method (Ref 2) was published.

Theodorsen made use of the fact that any closed curve, such as an airfoil, defined in the complex plane, may be transformed mathematically into a circle. This transformation may be further required to be conformal; that is, to preserve the local angular relationship between lines passing through each point. Conformality, therefore, ensures that the angle of attack of the airflow is unaffected by the transformation. The problem then becomes that of analyzing the two-dimensional flow over a circle. Since this is one of the very few cases for which exact solutions to the equations of motion are known, the velocity at each point

on the circle may be obtained immediately. Then, through an inverse transformation, the potential flow velocity at the corresponding point on the surface of the airfoil may also be determined. This velocity may be used as an approximation, (since boundary layer thickness has not yet been accounted for) to the velocity at the edge of the boundary layer.

Straightforward though this method appears, its use before the advent of high-speed computers was limited in practice by the enormity of the task of solving the necessary integral equations iteratively to the desired accuracy. The transformation is very time-consuming and tedious when performed by hand, providing numerous opportunities to make minor mathematical errors which may invalidate subsequent work. Since these are precisely the disadvantages in computation that a digital computer is designed to overcome, Theodorsen's method lends itself well to formulation for machine use.

The rate at which the iterative solution converges is largely dependent upon how nearly the original airfoil approximates a circle. Therefore, Theodorsen recommends the use of an intermediate analytical transformation (the Joukowski transformation) which converts the airfoil shape into a pseudo-circle conformally, and, thereby, reduces the computation time required.

Boundary Layer Region

The boundary layer equations may be derived from the Navier-Stokes equations for viscous fluid motion under the assumptions of steady, incompressible, constant viscosity flow at large Reynold's numbers. The Karman-Pohlhausen method (Ref 3) of solving the boundary layer equations is based on the further assumption that the velocity profile may be adequately represented as a fourth-degree polynomial satisfying appropriate boundary conditions, including the edge velocity distribution previously found from Theodorsen's method.

Combined Flow Fields

The boundary layer flow determined from the Karman-Pohlhausen method is only a first approximation, because a body with a boundary layer appears to the potential flow to be thicker by the amount of the displacement thickness. Therefore, the displacement thickness of the boundary layer must be computed for the approximate edge velocity; then this thickness must be added to the actual thickness of the body; and the inviscid velocity field for the resulting shape determined by Theodorsen's method. Thus, the velocity field solutions are continually refined until the change in displacement thickness from one iteration to the next is negligible. At this point, the problem of finding the velocity field may be considered solved. With the velocity field known, other aerodynamic parameters such as lift,

drag, circulation, and separation point may also be computed, using standard methods.

## II. Theodorsen's Method

### Method of Presentation

Theodorsen's method of irrotational flow analysis depends upon several important results of potential theory and the theory of conformal transformations of complex functions. These results will be briefly summarized before a detailed presentation of the Joukowski and Theodorsen transformations is given. Finally, the process for obtaining surface velocities by an inverse transformation will be presented.

### Review of Potential Theory

The flow outside the boundary layer is assumed to be steady, irrotational, and incompressible, permitting its description in terms of a velocity potential  $\phi$  or a stream function  $\psi$ , defined so that:

$$u = \frac{\partial \phi}{\partial x} = \frac{\partial \psi}{\partial y} \quad \text{velocity in x-direction} \quad (1)$$

$$v = \frac{\partial \phi}{\partial y} = - \frac{\partial \psi}{\partial x} \quad \text{velocity in y-direction}$$

The lines of constant  $\psi$  (streamlines) and lines of constant  $\phi$  (equipotential lines) are orthogonal families of curves.

Any functions of  $\phi$  and  $\psi$  which satisfy Laplace's equation,  $\nabla^2 \phi = \nabla^2 \psi = 0$ , represent possible types of fluid motion. The boundary conditions of impermeability of the airfoil surface and uniform flow at infinity define a unique solution.

Conformal Transformation

If  $w(\zeta) = \phi(x,y) + i\psi(x,y)$  is an analytic function of the complex variable  $\zeta = x + iy$ , and the components  $\phi$  and  $\psi$  satisfy Laplace's equation, then certain useful relations exist between the  $\zeta$ -plane and the  $w$ -plane. Specifically, any simple curve  $f(\zeta)$ , such as an airfoil surface, maps into a curve  $f(w)$  in the  $w$ -plane in such a manner that the angles between pairs of lines passing through any point in the  $\zeta$ -plane remain unchanged at the image point in the  $w$ -plane, although local rotations and magnifications may occur. Therefore, the streamlines and equipotential lines of the  $\zeta$ -plane remain orthogonal in the plane of transformation. An exception occurs at points where  $\frac{dw}{d\zeta} = 0$ . These points correspond to flow stagnation points in the exact circle plane, and also in the airfoil plane, unless the trailing edge is cusped, in which case the airfoil has no trailing edge stagnation point.

Riemann has shown that the transformed curve may be specified without negating the conformal characteristic of the transformation. In particular, the interior of any simply-connected region can be mapped inside a circle, with the curve enclosing the region mapping onto the circumference of the circle. This transformation is unique when the origins and orientations of the coordinate systems in the two planes are specified.

Joukowski Transformation

The transformation  $\zeta = z' + a^2/z'$ , where the  $\zeta$ -plane is the plane of the airfoil ( $\zeta = x + iy$ ) is the Joukowski transformation. If the airfoil is elliptical or one of the special class of airfoils known as Joukowski airfoils, then a circle results in the  $z'$ -plane. If not, then a curve (pseudo-circle in Fig. 1) closely approximating a circle results for conventional airfoil shapes. While this transformation is not essential to Theodorsen's method, it improves the rate of convergence of the subsequent transformation. The constant "a" is included to preserve dimensions and has the dimension of length. The curve in the  $z'$ -plane can also be represented as  $z' = ae^{\psi+i\omega}$  in polar coordinates, where  $\rho = ae^{\psi}$  is the radius vector and the angular coordinate is  $\omega$ . Substituting the polar form of  $z'$  into the transformation equation yields

$$\zeta = 2a \cosh (\psi + i\omega) \quad (2)$$

or

$$\zeta = 2a \cosh \psi \cos \omega + 2ia \sinh \psi \sin \omega \quad (3)$$

Noting that  $\zeta = x + iy$ , and equating real and imaginary parts, the airfoil coordinates may be found explicitly in terms of the transformation coordinates

$$x = 2a \cosh \psi \cos \omega$$

$$y = 2a \sinh \psi \sin \omega \quad (4)$$

The inverse relations between coordinates will now be determined. Solving Eqs (4) for  $\cosh \psi$  and  $\sinh \psi$  and substituting into the identity  $\cosh^2 \psi - \sinh^2 \psi = 1$  gives

$$\left(\frac{x}{2a \cos \omega}\right)^2 - \left(\frac{y}{2a \sin \omega}\right)^2 = 1 \quad (5)$$

which can be solved for  $\omega$

$$\omega = \sin^{-1} \sqrt{1/2 \{n + \sqrt{n^2 + (y/a)^2}\}} \quad (6)$$

where

$$n = 1 - \left(\frac{x^2 + y^2}{4a^2}\right)$$

Likewise, Eqs (4) may be solved for  $\cos \omega$  and  $\sin \omega$  and substituted into the identity  $\cos^2 \omega + \sin^2 \omega = 1$ , giving

$$\left(\frac{x}{2a \cosh \psi}\right)^2 + \left(\frac{y}{2a \sinh \psi}\right)^2 = 1 \quad (7)$$

so that,

$$\psi = \sinh^{-1} \sqrt{1/2 \{-n + \sqrt{n^2 + (y/a)^2}\}} \quad (8)$$

#### Theodorsen Transformation

$$\sum_{n=0}^{\infty} \frac{C_n}{z^n}$$

The Theodorsen transformation  $z' = z e$  maps the pseudo-circle in the  $z'$ -plane into an exact circle (Fig. 1) in the  $z$ -plane. The coefficients  $C_n$  are complex numbers of the form  $A_n + iB_n$ . The condition that the flow at infinity

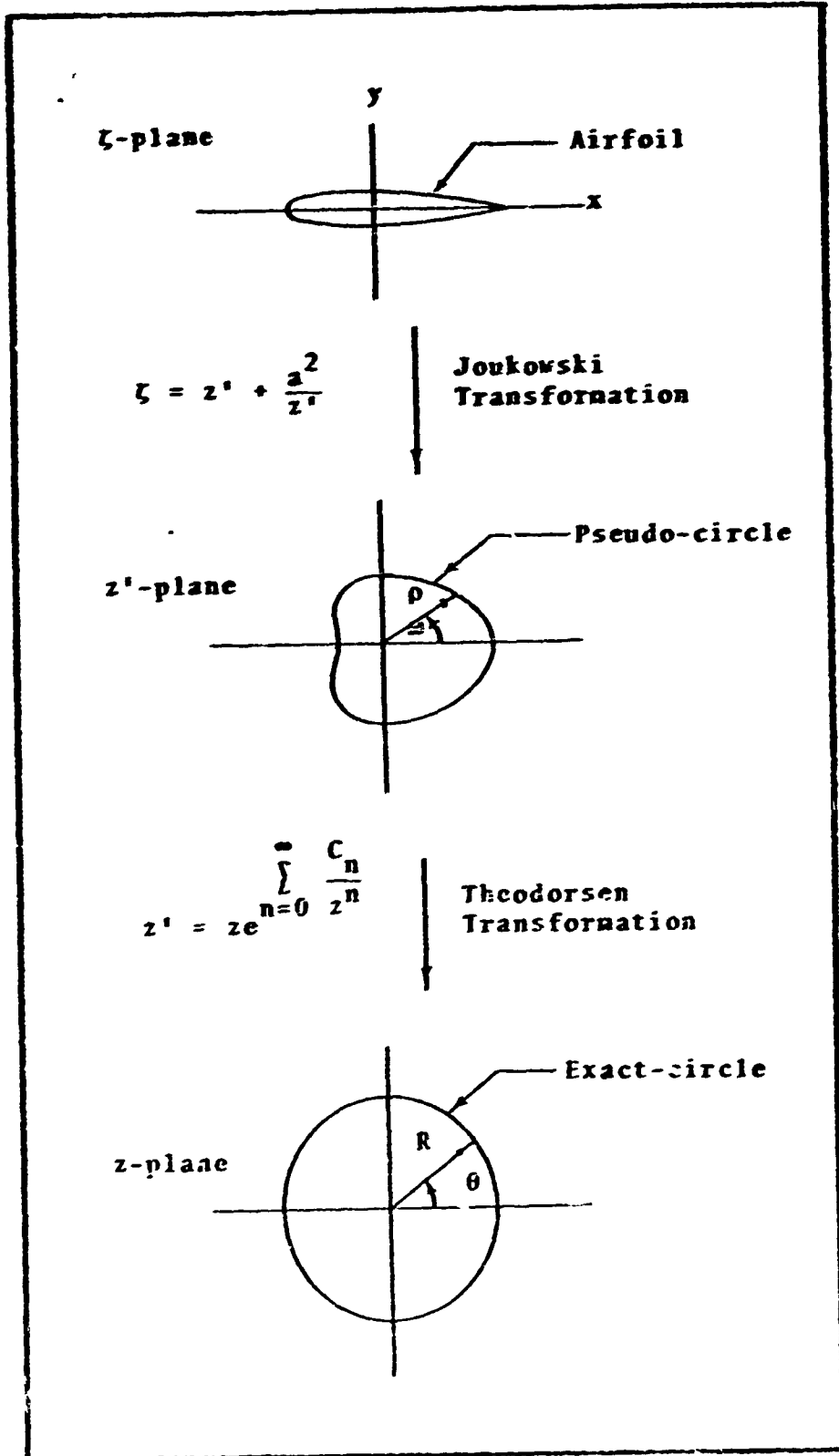


Fig. 1. Transformation Planes and Notation.

must be identical in airfoil and exact circle planes requires that  $A_0 = B_0 = 0$ . The transformation then becomes

$$z' = z e^{\sum_{n=1}^{\infty} \frac{C_n}{z^n}} = z e^{\sum_{n=1}^{\infty} \frac{A_n + iB_n}{z^n}} \quad (9)$$

Suitable means must now be found for determining the constants  $A_n$  and  $B_n$ .

The equation for the exact circle may be expressed as  $z = ae^{\phi+i\theta}$  in polar coordinates where  $\phi$  is a constant and  $R = ae^{\phi}$  is the radius vector and the angular coordinate is  $\theta$ . Eliminating the constant "a" between the polar definitions of  $z$  and  $z'$  yields

$$z' = z e^{(\psi-\phi) + i(\omega-\theta)} \quad (10)$$

Now, combining with the transformation equation

$$(\psi-\phi) + i(\omega-\theta) = \sum_{n=1}^{\infty} \frac{A_n + iB_n}{z^n} \quad (11)$$

Note that

$$z^n = (ae^{\phi+i\theta})^n = [R(\cos \theta + i \sin \theta)]^n = \frac{R^n}{\cos n\theta - i \sin n\theta} \quad (12)$$

Substituting into Eq (11)

$$(\psi - \phi) + i(\omega - \theta) = \sum_{n=1}^{\infty} \frac{A_n + iB_n}{R^n} (\cos n\theta - i \sin n\theta) \quad (13)$$

expanding

$$\begin{aligned} (\psi - \phi) + i(\omega - \theta) = \sum_{n=1}^{\infty} \left[ \frac{A_n}{R^n} \cos n\theta + \frac{B_n}{R^n} \sin n\theta \right] + \\ + i \sum_{n=1}^{\infty} \left[ \frac{B_n}{R^n} \cos n\theta - \frac{A_n}{R^n} \sin n\theta \right] \end{aligned} \quad (14)$$

and equating real and imaginary parts of Eq (14) establishes the following conjugate Fourier expansions:

$$\psi - \phi = \sum_{n=1}^{\infty} \left[ \frac{A_n}{R^n} \cos n\theta + \frac{B_n}{R^n} \sin n\theta \right] \quad (15)$$

$$\omega - \theta = \sum_{n=1}^{\infty} \left[ \frac{B_n}{R^n} \cos n\theta - \frac{A_n}{R^n} \sin n\theta \right] \quad (16)$$

The Fourier coefficients  $\frac{A_n}{R^n}$ ,  $\frac{B_n}{R^n}$ , and  $\phi$  (the constant term) of Eq (15) are given by

$$\frac{A_n}{R^n} = \frac{1}{\pi} \int_0^{2\pi} \bar{\psi}(\lambda) \cos n\lambda \, d\lambda \quad (17)$$

$$\frac{B_n}{R^n} = \frac{1}{\pi} \int_0^{2\pi} \bar{\psi}(\lambda) \sin n\lambda \, d\lambda \quad (18)$$

$$\phi = \frac{1}{2\pi} \int_0^{2\pi} \bar{\psi}(\lambda) \, d\lambda \quad (19)$$

where  $\lambda$  is an angular measure corresponding to  $\theta$  and  $\bar{\psi}(\lambda) = \psi[\omega(\lambda)]$ , since  $\psi$  is known only as a function of  $\omega$ . Therefore, a relation between  $\psi$  and  $\theta$  (or  $\lambda$ ) must be found. For any particular value of  $\theta$ , the coefficients given in Eqs (17) and (18) may be substituted into Eq (16), thereby eliminating these coefficients from that relation

$$\omega - \theta = \frac{1}{\pi} \sum_{n=1}^{\infty} \left[ \cos n\theta \int_0^{2\pi} \bar{\psi}(\lambda) \sin n\lambda \, d\lambda - \sin n\theta \int_0^{2\pi} \bar{\psi}(\lambda) \cos n\lambda \, d\lambda \right] \quad (20)$$

which reduces to

$$\omega - \theta = \frac{1}{\pi} \sum_{n=1}^{\infty} \left[ \int_0^{2\pi} \bar{\psi}(\lambda) \sin n(\lambda - \theta) \, d\lambda \right] = \frac{1}{\pi} \int_0^{2\pi} \bar{\psi}(\lambda) \left[ \sum_{n=1}^{\infty} \sin n(\lambda - \theta) \, d\lambda \right] \quad (21)$$

But,

$$\sum_{n=1}^N \sin n(\lambda - \theta) = \frac{1}{2} \cot \frac{\lambda - \theta}{2} - \frac{\cos \left[ (2N+1) \frac{\lambda - \theta}{2} \right]}{2 \sin \frac{\lambda - \theta}{2}} \quad (22)$$

so that

$$\omega - \theta = \lim_{N \rightarrow \infty} \left[ \frac{1}{2\pi} \int_0^{2\pi} \bar{\psi}(\lambda) \cot \frac{\lambda - \theta}{2} d\lambda - \frac{1}{2\pi} \int_0^{2\pi} \bar{\psi}(\lambda) \frac{\cos \left[ (2N+1) \frac{\lambda - \theta}{2} \right]}{2 \sin \frac{\lambda - \theta}{2}} d\lambda \right] \quad (24)$$

Since the second term is identically zero and the first one is unaffected in the limit,

$$\omega - \theta = \frac{1}{2\pi} \int_0^{2\pi} \bar{\psi}(\lambda) \cot \frac{\lambda - \theta}{2} d\lambda \quad (25)$$

The difference,  $(\omega - \theta)$  or  $(\omega - \lambda)$ , between angular coordinates of a point and its image in the pseudo-circle and exact circle planes is called the conformal angular distortion function, and is denoted by  $\epsilon$ , so that

$$\epsilon(\theta) = \frac{1}{2\pi} \int_0^{2\pi} \psi[\epsilon(\lambda) + \lambda] \cot \frac{\lambda - \theta}{2} d\lambda \quad (26)$$

Equation (26) is of fundamental importance in the practical application of Theodorsen's method, as it may be solved iteratively for  $\epsilon(\theta)$ , from which  $\omega(\theta)$  is obtained permitting the solution of Eq (19) for the constant  $\phi$ . Note that the relationship between polar coordinates in the pseudo-circle and exact circle planes has been obtained without having to solve for the Fourier coefficients directly.

Surface Velocity

It is shown in potential flow theory that the complex velocity potential for a circle in the  $z$ -plane immersed in steady,  $x$ -directed flow is

$$w(z) = \phi + i\psi = -V_{\infty} \left( z + \frac{R^2}{z} \right) - \frac{i\Gamma}{2\pi} \ln \frac{z}{R} \quad (27)$$

where  $V_{\infty}$  is the freestream velocity,  $R = ae^{\phi}$  is the radius of the circle, and  $\Gamma$  is the circulation. The fluid velocity in the circle plane is obtained by differentiating  $w(z)$

$$V(z) = \frac{dw}{dz} = u + iv = -V_{\infty} \left( 1 - \frac{R^2}{z^2} \right) - \frac{i\Gamma}{2\pi z} \quad (28)$$

This velocity will be zero ( $u = v = 0$ ) at stagnation points. Therefore, the locations ( $z_0$ ) of these points is given by the value for  $z$  when  $\frac{dw}{dz} = 0$ . That is,

$$z_0 = \frac{-i\Gamma \pm \sqrt{16\pi^2 R^2 V_{\infty}^2 - \Gamma^2}}{4\pi V_{\infty}} \quad (29)$$

A non-zero angle of attack  $\alpha$  may be accounted for by replacing  $z$  by  $ze^{i\alpha}$  in the real part of Eq (27). This has the effect of rotating the flow field about the circle by the angle  $\alpha$ .

$$w(z) = -V_{\infty} \left( ze^{i\alpha} + \frac{R^2}{z} e^{-i\alpha} \right) - \frac{i\Gamma}{2\pi} \ln z \quad (30)$$

and

$$V(z) = -V_{\infty} e^{i\alpha} \left( 1 - \frac{R^2}{z^2} e^{-2i\alpha} \right) - \frac{i\Gamma}{2\pi z} \quad (31)$$

The well-known Kutta-Joukowski condition requires that the trailing edge ( $\omega = \pi$ ) on an airfoil which does not have a cusped trailing edge be a stagnation point in order that infinite velocities and pressure gradients may be avoided. The circulation required to meet this condition may be found by setting  $z_0 = Re^{i(\pi+\beta)} = -Re^{i\beta}$  (where  $\beta$  is the negative of the value of  $\epsilon$  at  $\omega = \pi$ , and is called the angle of zero lift for the airfoil) and  $V(z) = 0$  in Eq (31), and solving for the corresponding  $\Gamma$ :

$$\Gamma = 4\pi R V_{\infty} \sin(\alpha + \beta) \quad (32)$$

Then

$$V(z) = \frac{dw}{dz} = -V_{\infty} e^{i\alpha} \left( 1 - \frac{R^2}{z^2} e^{-2i\alpha} \right) - i \frac{4\pi R V_{\infty} \sin(\alpha + \beta)}{2\pi z} \quad (33)$$

The velocity,  $v(z)$ , in the plane of the circle must now be converted to the velocity,  $v(\zeta)$ , at the surface of the airfoil through the use of transformation derivatives:

$$v(\zeta) = \left| \frac{dw}{d\zeta} \right| = \left| \frac{dw}{dz} \right| \left| \frac{dz}{dz'} \right| \left| \frac{dz'}{d\zeta} \right| \quad (34)$$

and these derivatives must now be determined. Recall that  $z = Re^{i\theta}$  on the surface of the circle. Substituting this

value for  $z$  in Eq (33) gives

$$\frac{dw}{dz} = -V_0 e^{i\alpha} [1 - e^{-2i(\alpha+\theta)}] - 2iV_0 e^{-i\theta} \sin(\alpha+\beta) \quad (35)$$

which reduces to

$$\frac{dw}{dz} = -2iV_0 e^{-i\theta} [\sin(\alpha+\theta) + \sin(\alpha+\beta)] \quad (36)$$

the absolute value of which is

$$\left| \frac{dw}{dz} \right| = 2V_0 [\sin(\alpha+\theta) + \sin(\alpha+\beta)] \quad (37)$$

From the definitions of  $z$ ,  $z'$ , and  $\epsilon$

$$\frac{z'}{z} = \frac{ze^{\psi+i\omega}}{ae^{\phi+i\theta}} = e^{(\psi-\theta)+i\epsilon} \quad (38)$$

Differentiating and noting that  $\phi$  is a constant

$$\begin{aligned} \frac{dz'}{dz} &= e^{(\psi-\phi)+i\epsilon} + ze^{(\psi-\phi)+i\epsilon} \frac{d}{dz} [(\psi-\phi)+i\epsilon] = \\ &= \frac{z'}{z} \left[ 1 + z \frac{d}{dz} (\psi+i\epsilon) \right] \end{aligned} \quad (39)$$

But

$$\frac{1}{z} dz = \frac{1}{ae^{\phi+i\theta}} d(ae^{\phi+i\theta}) = i d\theta \quad (40)$$

Substitution into Eq (39) gives

$$\frac{dz'}{dz} = \frac{z'}{z} \left[ 1 + \frac{d(\psi+i\epsilon)}{i d\theta} \right] = \frac{z'}{z} \left( 1 - i \frac{d\psi}{d\theta} + \frac{d\epsilon}{d\theta} \right) \quad (41)$$

Further algebraic manipulation on this equation gives

$$\frac{dz'}{dz} = \frac{z'}{z} \left[ \frac{(d\theta/d\omega) + (d\epsilon/d\omega) - i (d\psi/d\omega)}{(d\theta/d\omega)} \right] \quad (42)$$

Applying the definition  $\epsilon = \omega - \theta$ , and reducing

$$\frac{dz'}{dz} = \frac{z'}{z} \left[ \frac{1 - i (d\psi/d\omega)}{1 - (d\epsilon/d\omega)} \right] \quad (43)$$

And finding the absolute value

$$\left| \frac{dz'}{dz} \right| = e^{\psi-\phi} \left[ \frac{\sqrt{1 + (d\psi/d\omega)^2}}{1 - (d\epsilon/d\omega)} \right] \quad (44)$$

Inverting

$$\left| \frac{dz}{dz'} \right| = e^{\phi-\psi} \left[ \frac{1 - (d\epsilon/d\omega)}{\sqrt{1 + (d\psi/d\omega)^2}} \right] \quad (45)$$

which is the desired derivative. Substituting the definition

$z' = ae^{\psi+i\omega}$  into the Joukowski transformation

$$\zeta = ae^{\psi+i\omega} + ae^{-\psi-i\omega} = 2a \cosh (\psi+i\omega) \quad (46)$$

Differentiating

$$\frac{d\zeta}{dz'} = 2 \sinh (\psi+i\omega) e^{-\psi-i\omega} \quad (47)$$

Expanding

$$\frac{d\zeta}{dz'} = 2e^{-\psi-i\omega} (\sinh \psi \cosh i\omega + \cosh \psi \sinh i\omega) \quad (48)$$

Noting that  $\cosh i\omega = \cos \omega$  and  $\sinh i\omega = i \sin \omega$ , this becomes

$$\frac{d\zeta}{dz'} = 2e^{-\psi-i\omega} (\sinh \psi \cos \omega + i \cosh \psi \sin \omega) \quad (49)$$

Then

$$\left| \frac{d\zeta}{dz'} \right|^2 = 4e^{-2\psi} (\sinh^2 \psi \cos^2 \omega + \cosh^2 \psi \sin^2 \omega) \quad (50)$$

which reduces to

$$\left| \frac{d\zeta}{dz'} \right|^2 = 4e^{-2\psi} (\sinh^2 \psi + \sin^2 \omega) \quad (51)$$

Taking the square root and inverting gives the final derivative

$$\left| \frac{dz'}{d\zeta} \right| = \frac{e^{\psi}}{2\sqrt{\sinh^2 \psi + \sin^2 \omega}} \quad (52)$$

The derivatives given in Eqs (37), (45), and (52) will now be substituted into Eq (34) to find the airfoil surface velocity

$$V(\zeta) = \frac{V_{\infty} e^{\phi} [\sin(\alpha+\theta) + \sin(\alpha+\beta)] [1 - (d\epsilon/d\omega)]}{\sqrt{(\sinh^2 \psi + \sin^2 \omega) [1 + (d\psi/d\omega)^2]}} \quad (53)$$

This is the velocity which will then be used as an approximation for the edge velocity in the analysis of the boundary layer.

### III. Karman-Pohlhausen Method

#### Origin

General motion of a viscous fluid is described by the Navier-Stokes equations, which were derived from first principles. Schlichting (Ref 3) has shown that, if Reynolds number is large, viscosity is constant, and flow is steady and incompressible, then the equations of motion for flow over a surface may be approximated by the momentum integral equation:

$$U^2 \frac{d\delta_2}{dx} + (2\delta_2 + \delta_1) U \frac{dU}{dx} = \frac{\tau_w}{\rho} \quad (54)$$

where the boundary layer displacement and momentum thicknesses are, respectively,

$$\delta_1 = \int_0^{\infty} \left( 1 - \frac{u}{U} \right) dy \quad (55)$$

$$\delta_2 = \int_0^{\infty} \frac{u}{U} \left( 1 - \frac{u}{U} \right) dy \quad (56)$$

and where  $x$  and  $y$  are, respectively, the streamwise and cross-stream coordinates of a general point in the flow (Fig. 2), with the corresponding velocities given by  $u$  and  $v$ . Note that the boundary layer edge velocity  $U$  is a parameter common to both the potential flow and boundary layer regions.

The following analysis is due originally to Pohlhausen, but is presented in the form developed by Holstein and

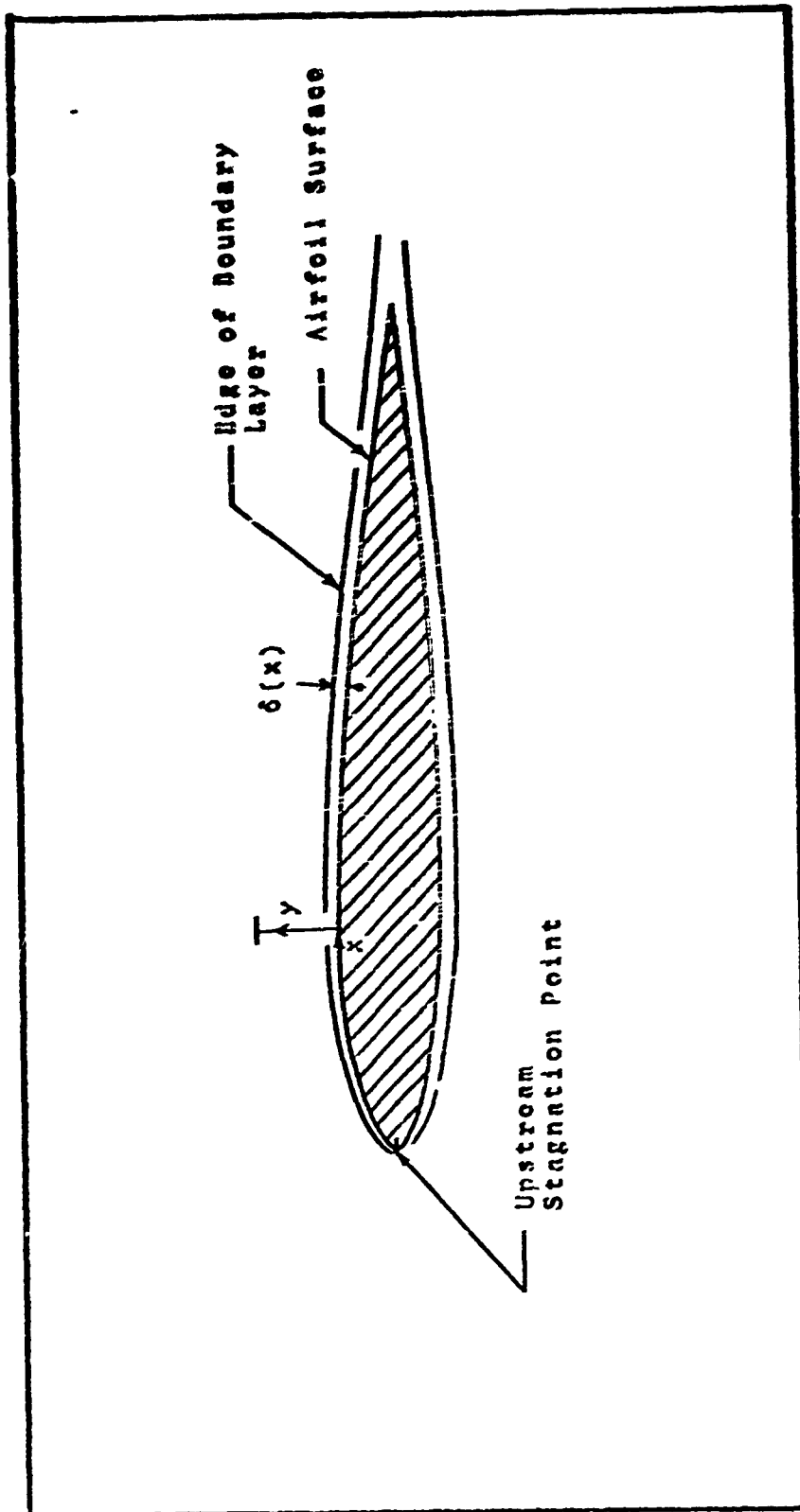


FIG. 2. Boundary Layer Coordinate System.

Bohlen, and described by Schlichting.

### Velocity Profile

A velocity profile of the following form is now assumed:

$$\frac{u}{U} = a\eta + b\eta^2 + c\eta^3 + d\eta^4 \quad (57)$$

where  $\eta = y/\delta$  and  $a$ ,  $b$ ,  $c$ , and  $d$  are coefficients to be determined.

Observations indicate that the following boundary conditions should be applied to the solution of Eq (54):

$$u = 0 \quad \text{at } y = 0 \quad (58)$$

$$v \frac{\partial^2 u}{\partial y^2} = -U \frac{dU}{dx} \quad \text{at } y = 0 \quad (59)$$

$$u = U \quad \text{at } y = \delta \quad (60)$$

$$\frac{\partial u}{\partial y} = 0 \quad \text{at } y = \delta \quad (61)$$

$$\frac{\partial^2 u}{\partial y^2} = 0 \quad \text{at } y = \delta \quad (62)$$

where  $\delta$ , called the boundary layer thickness, is the cross-stream distance from the surface at which the boundary layer meets the potential flow region.

Note that the first boundary condition, Eq (58), is identically satisfied by the assumed solution by virtue of the omission of a constant term in the polynomial. There remain, therefore, four boundary conditions to determine

a, b, c, and d. In terms of the assumed velocity profile, the second through fifth boundary conditions become, respectively,-

$$Uv \left[ \frac{\partial^2}{\partial \eta^2} \left( \frac{u}{U} \right) \left( \frac{\partial \eta}{\partial y} \right)^2 \right] = -U \frac{dU}{dx} \quad \text{at } \eta = 0 \quad (63)$$

$$\frac{u}{U} = 1 \quad \text{at } \eta = 1 \quad (64)$$

$$U \left[ \frac{\partial}{\partial \eta} \left( \frac{u}{U} \frac{\partial \eta}{\partial y} \right) \right] = 0 \quad \text{at } \eta = 1 \quad (65)$$

$$U \left[ \frac{\partial^2}{\partial \eta^2} \left( \frac{u}{U} \right) \left( \frac{\partial \eta}{\partial y} \right)^2 \right] = 0 \quad \text{at } \eta = 1 \quad (66)$$

Application of these conditions to the assumed solution and defining a shape factor

$$\Lambda = \frac{\delta^2}{v} \frac{dU}{dx} \quad (67)$$

leads to the following expression for the velocity profile:

$$\frac{u}{U} = (2\eta - 2\eta^3 + \eta^4) + \frac{\Lambda}{6} (\eta - 3\eta^2 + 3\eta^3 - \eta^4) \quad (68)$$

By applying the physical constraints that  $\frac{\partial u}{\partial y} = 0$  at  $y = 0$  at the separation point and that  $\frac{u}{U} \leq 1$  within the boundary layer, the upper and lower physical limits on  $\Lambda$  are readily determined. These have been found to be +12 and -12, respectively.

Other Parameters

The displacement thickness, momentum thickness, and shear stress will now be found in terms of  $\Lambda$ .

Substituting the above velocity profile and the definition for  $\eta$  into the definition for displacement thickness given by Eq (55) gives

$$\frac{\delta_1}{\delta} = \int_0^1 [1 - (2\eta - 2\eta^3 + \eta^4) - \frac{\Lambda}{6} (\eta - 3\eta^2 + 3\eta^3 - \eta^4)] d\eta \quad (69)$$

And, finally,

$$\frac{\delta_1}{\delta} = \frac{3}{10} - \frac{\Lambda}{120} \quad (70)$$

Likewise,

$$\frac{\delta_2}{\delta} = \frac{37}{315} - \frac{\Lambda}{945} - \frac{\Lambda^2}{9072} \quad (71)$$

Now, the shear stress, by definition, is

$$\tau_w = \mu \left. \frac{\partial u}{\partial y} \right|_{y=0} \quad (72)$$

Evaluating the derivative and multiplying both sides by  $\frac{\delta}{\mu U}$ , gives

$$\frac{\tau_w \delta}{\mu U} = 2 + \frac{\Lambda}{6} \quad (73)$$

Simplification of Momentum Integral Equation

The momentum integral equation can now be put into a form from which practical results may be obtained.

Multiplying both sides of Eq (54) by  $\frac{\delta_2}{v}$ , and reducing, leads to

$$\frac{\tau_w \delta_2}{\rho U} = \frac{U}{v} \delta_2 \frac{d\delta_2}{dx} + \left(2 + \frac{\delta_1}{\delta_2}\right) \frac{\delta_2^2}{v} \frac{dU}{dx} \quad (74)$$

Equations (67), (68), (70), (71), and (74), together with the known edge velocity distribution, form a solvable system. However, elimination of dependence of the other variables on  $\delta$  is desirable, since the boundary layer thickness is physically meaningless. Furthermore, the  $\frac{d\delta_2}{dx}$  quantity in Eq (74) leads to a requirement for  $\frac{d^2U}{dx^2}$  at every point on the surface. By suitable mathematical manipulation, this can be reduced to a requirement for  $\frac{d^2U}{dx^2}$  at the upstream stagnation point only. The following analysis proceeds, therefore, toward these objectives.

Introduction of several new parameters will permit simplification of the form of Eq (74). Define

$$K = \frac{\delta_2^2}{v} \frac{dU}{dx} \quad (75)$$

Then,

$$K = \left(\frac{\delta_2}{\delta}\right)^2 \frac{\delta^2}{v} \frac{dU}{dx} = \Lambda \left(\frac{\delta_2}{\delta}\right)^2 = \Lambda \left(\frac{37}{315} - \frac{\Lambda}{945} - \frac{\Lambda^2}{9072}\right)^2 \quad (76)$$

Let

$$z = \frac{\delta_2^2}{\nu} \quad (77)$$

So that

$$\frac{dz}{dx} = \frac{2}{\nu} \delta_2 \frac{d\delta_2}{dx} \quad (78)$$

Also, from Eqs (75) and (77)

$$K = z \frac{dU}{dx} \quad (79)$$

The ratio of displacement to momentum boundary layer thicknesses may be defined

$$f_1 = \frac{\delta_1}{\delta_2} \quad (80)$$

Or, using Eqs (70) and (71)

$$f_1 = \frac{\frac{\delta_1}{\delta}}{\frac{\delta_2}{\delta}} = \frac{\frac{3}{10} - \frac{\Lambda}{120}}{\frac{37}{315} - \frac{f}{945} - \frac{\Lambda^2}{9072}} \quad (81)$$

And, finally, the definition

$$f_2 = \frac{\tau_w \delta_2}{\mu U} \quad (82)$$

gives, using Eqs (71) and (73),

$$f_2 = \frac{\tau_w \delta}{\mu U} \left( \frac{\delta_2}{\delta} \right) = \left( 2 + \frac{\Lambda}{6} \right) \left( \frac{37}{315} - \frac{\Lambda}{945} - \frac{\Lambda^2}{9072} \right) \quad (83)$$

Now, if these definitions are substituted into Eq (74), the result is

$$f_2 = \frac{U}{2} \frac{dZ}{dx} + (2 + f_1)K \quad (84)$$

which may be rearranged to give

$$U \frac{dZ}{dx} = 2f_2 - (4 + 2f_1)K \quad (85)$$

The right side of Eq (85) is a function of  $\Lambda$  alone, as shown by Eqs (76), (81), and (83). Therefore, if a new parameter  $F$  is defined such that

$$F = 2f_2 - (4 + 2f_1)K \quad (86)$$

Then, it may be shown that

$$F = 2 \left( \frac{37}{315} - \frac{\Lambda}{945} - \frac{\Lambda^2}{9072} \right) \left[ 2 - \frac{116}{315} \Lambda + \left( \frac{2}{945} + \frac{1}{120} \right) \Lambda^2 + \frac{2}{9072} \Lambda^3 \right] \quad (87)$$

And Eq (85), the equation of motion, becomes

$$\frac{dZ}{dx} = \frac{F}{U} \quad (88)$$

Conditions at Stagnation Point

Enough relations now exist to permit a stepwise solution for all the boundary layer parameters, once a starting condition is known. Starting conditions, therefore, will now be determined at the upstream stagnation point.

Since the flow is brought to rest at the stagnation point,  $U_0 = 0$  (where the "0" subscript means that an associated variable is to be evaluated at stagnation point conditions). Then, from Eq (88),  $F_0$  must also be zero if  $\left(\frac{dz}{dx}\right)\Big|_0$  is to exist. Therefore,  $\Lambda_0$  must be a root of Eq (87) when  $F = 0$ . The roots of this equation are -72.2, -37.8, 7.052, 17.9, and 28.2. Because of the physical limitations on the range of  $\Lambda$ , it may be seen that

$$\Lambda_0 = 7.052 \quad (89)$$

Then from Eq (76),

$$K_0 = .0770 \quad (90)$$

And, from Eq (79),

$$Z_0 = \frac{.0770}{\left(\frac{dU}{dx}\right)\Big|_0} \quad (91)$$

which determines  $Z_0$ , since the edge velocity distribution is known from the potential flow analysis.

Now,  $\left(\frac{dz}{dx}\right)\Big|_0$  may be found by applying L'Hospital's Rule to Eq (88)

$$\left( \frac{dZ}{dx} \right) \Big|_0 = \lim_{x \rightarrow 0} \left[ \frac{(dF/dx)}{(dU/dx)} \right] = \lim_{x \rightarrow 0} \left[ \frac{(dF/dK)(dK/dx)}{(dU/dx)} \right] \quad (92)$$

But, from Eq (79),

$$\frac{dK}{dx} = \frac{dZ}{dx} \frac{dU}{dx} + Z \frac{d^2U}{dx^2} \quad (93)$$

Substituting this expression into Eq (92) and passing to the limit gives

$$\left( \frac{dZ}{dx} \right) \Big|_0 = Z_0 \left[ \frac{\left( \frac{dF}{dK} \right) \Big|_0}{1 - \left( \frac{dF}{dK} \right) \Big|_0} \right] \left[ \frac{\left( \frac{d^2U}{dx^2} \right) \Big|_0}{\left( \frac{dU}{dx} \right) \Big|_0} \right] \quad (94)$$

But, using Eqs (76) and (87),

$$\left( \frac{dF}{dK} \right) \Big|_0 = \frac{\left( \frac{dF}{d\Lambda} \right) \Big|_0}{\left( \frac{dK}{d\Lambda} \right) \Big|_0} = -5.57 \quad (95)$$

Substituting the values for  $Z_0$  and  $\left( \frac{dF}{dK} \right) \Big|_0$  given by Eqs (91) and (95), respectively, into Eq (94) provides an expression for  $\left( \frac{dZ}{dx} \right) \Big|_0$  in terms of the edge velocity distribution:

$$\left( \frac{dZ}{dx} \right) \Big|_0 = -.0652 \frac{\left( \frac{d^2U}{dx^2} \right) \Big|_0}{\left( \frac{dU}{dx} \right) \Big|_0} \quad (96)$$

Using the Method

With starting conditions known at the stagnation point, the value for  $Z$  at a distance  $\Delta x$  downstream is

$$z_1 = z_0 + \left( \frac{dz}{dx} \right) \Big|_0 \Delta x \quad (97)$$

Then, from Eq (79),

$$K_1 = z_1 \left( \frac{dU}{dx} \right) \Big|_1 \quad (98)$$

The corresponding value of  $\Lambda$ , from Eq (76) may now be used to find  $F_1$  from Eq (87). Using Eq (88),

$$\left( \frac{dz}{dx} \right) \Big|_1 = \frac{F_1}{U_1} \quad (99)$$

so that the stepping process may be continued indefinitely, the value of  $Z$  at point "n" being

$$z_n = z_{n-1} + \left( \frac{dz}{dx} \right) \Big|_{n-1} \Delta x \quad (100)$$

Knowledge of  $\Lambda_n$  permits determination of  $f_{1n}$ ,  $f_{2n}$ , and the velocity profile  $\left( \frac{u}{U} \right) \Big|_n$ , using Eqs (45), (83), and (68), respectively. Substituting  $Z_n$  into Eq (77) yields  $\delta_{2n}$ , which in turn produces  $\tau_{wn}$  from Eq (82), and, the ultimate objective,  $\delta_{1n}$  from Eq (80). This value of  $\delta_{1n}$  must be added to the original airfoil thickness to form a better

approximation of the potential flow airfoil shape to be analyzed again by Theodorsen's method.

Limitation

The Karman-Pohlhausen method of boundary layer analysis does not properly describe the flow downstream of a separation point (the point at which the shear stress at the wall vanishes).

#### IV. Computer Study

##### Purpose of Computer Study

A Fortran Extended program for the CDC-6600 computer was written as part of this study and is listed in Appendix A. It implements the theory discussed in the preceding chapters and lays a foundation for more sophisticated airfoil analysis programs. Flow parameters from this program may be compared with those from simplified airfoil theories in order to determine the validity of thin airfoil and inviscid assumptions. Some pertinent facts about the program will be discussed in this chapter.

##### Program Composition

The computer program is composed of a main program and several subprograms and functions. The main program is called MAGIC and provides the means for reading input data, controlling data flow and sequencing among subprograms, and testing for completion of the iteration on displacement thickness. One principal subprogram is THEO, which applies Theodorsen's method to the airfoil; the other is BOUND, which solves the boundary layer equations using the Karman-Pohlhausen method. Other subprograms and their purposes include: FNEVAL, which defines integrands; SIMPS, which performs integrations using Simpson's Rule; MTXEQ, which solves systems of algebraic equations; PLSQ, a polynomial least-square curve-fitting routine; ATKN, an interpolating function; several subroutines for the CALCOMP plotter; and

numerous standard functions from the system library.

### Input

Program MAGIC requires an alphanumeric description of the airfoil (e.g., NACA 1408), the number of data points, the Cartesian coordinates of each point, a plotting index, freestream velocity, viscosity, density, and the angle of attack on the chord line. The airfoil chord line is assumed to lie on the x-axis with the trailing edge in the positive x-direction and the midchord point at the origin. Points defining the airfoil surface must begin at the trailing edge and be numbered in the counterclockwise direction. All dimensions must be referenced to chord length. The plotting index causes the airfoil and its transformations in sub-program THEO: (1) to be plotted on the same axes, (2) not to be plotted, or (3) to be plotted on separate axes, according as its value is -1, 0, or +1, respectively. The angle of attack must be given in degrees.

Additionally, accuracy requirements on various computations may be reset by modifications to the program.

### Output

Program MAGIC computes and prints Cartesian coordinates in all three planes, polar coordinates in the pseudo-circle and exact circle planes, potential flow surface velocity, coefficients for fifth-order polynomials for  $\bar{\psi}(\theta)$  and  $\psi(\omega)$ , radius of exact circle, zero-lift angle of attack, circulation, section lift, pressure coefficients, shear stress at

surface, momentum thickness, displacement thickness, shape factor, and several important quantities used in computing these. The airfoil surface in all three planes is plotted (provided that the plotting index is non-zero), as are pressure coefficient, shear stress, and displacement thickness as functions of chordwise station. Samples of output format are shown in Appendix A.

#### Limitations on Program

Although subprogram THEO gives correct results for non-zero angles of attack, subprogram BOUND does not, since the shift of upstream stagnation point with angle of attack has not been accounted for. Therefore, accurate results for the complete program may be expected only for zero angle of attack.

Values of shear stress and displacement thickness generated by subprogram BOUND downstream of the separation point become very large. These values are printed as output, but are actually limited to a reasonable maximum value before being plotted or transmitted to subprogram THEO for another iteration. In particular, the displacement thickness at the trailing edge is set to zero in order that the new airfoil shape considered by subprogram THEO will be a closed curve.

## V. Results

### Conformal Transformations

Transformations were accomplished by subprogram THEO on several airfoils, including NACA 1408 and NACA 4424. The output plot of the transformation on the NACA 4424 airfoil is presented in Fig. 3. Success of the transformation on these airfoils was measured by the accuracy of the output angle of zero lift,  $\beta$ . The values for these angles as given by Abbott and von Doenhoff (Ref 1) are presented for comparison in Table 1. Comparison data was not available for the other airfoils used.

Table 1

#### Comparison of Zero Lift Angles of Attack

<u>Airfoil</u>	<u>(Program HAGIC)</u>	<u>(Ref 5)</u>
NACA 1408	.95°	.95°
NACA 4424	3.58°	3.50°

### Potential Flow Surface Velocities

Surface velocities generated by subprogram THEO were also compared with those given by Abbott and von Doenhoff. A typical comparison is shown in Table 2. The velocities agree within 2% in most cases. Exceptions occur at points where the radius of curvature is relatively small; that is, near the leading edge. This probably reflects poor accuracies in numerical derivatives in that area.

Table 2

Comparison of Potential Flow Velocities  
for XACA 1408 Airfoil

Upper Surface			Lower Surface		
Chordwise Station (percent chord)	$V/V_\infty$ (Program MAGIC)	$V/V_\infty$ (Ref 1)	Chordwise Station (Percent chord)	$V/V_\infty$ (Program MAGIC)	$V/V_\infty$ (Ref 1)
0	0	0	0	0	0
1.189	.780	1.061	1.311	.829	1.039
2.413	1.067	1.121	2.582	1.079	1.089
4.896	1.135	1.151	5.104	1.121	1.105
7.386	1.142	1.161	7.614	1.112	1.105
9.883	1.145	1.161	10.117	1.102	1.099
14.889	1.153	1.164	15.111	1.096	1.092
19.904	1.152	1.162	20.096	1.085	1.082
24.926	1.148	1.157	25.074	1.075	1.071
29.950	1.139	1.149	30.050	1.065	1.063
40.000	1.126	1.131	40.000	1.054	1.047
50.020	1.107	1.110	49.980	1.038	1.034
60.034	1.087	1.089	59.966	1.023	1.019
70.041	1.067	1.070	69.959	1.012	1.008
80.039	1.042	1.043	79.961	.998	.991
90.027	1.014	1.003	89.973	.982	.965
95.016	.966	.983	94.984	.953	.955
100.000	0	0	100.000	0	0

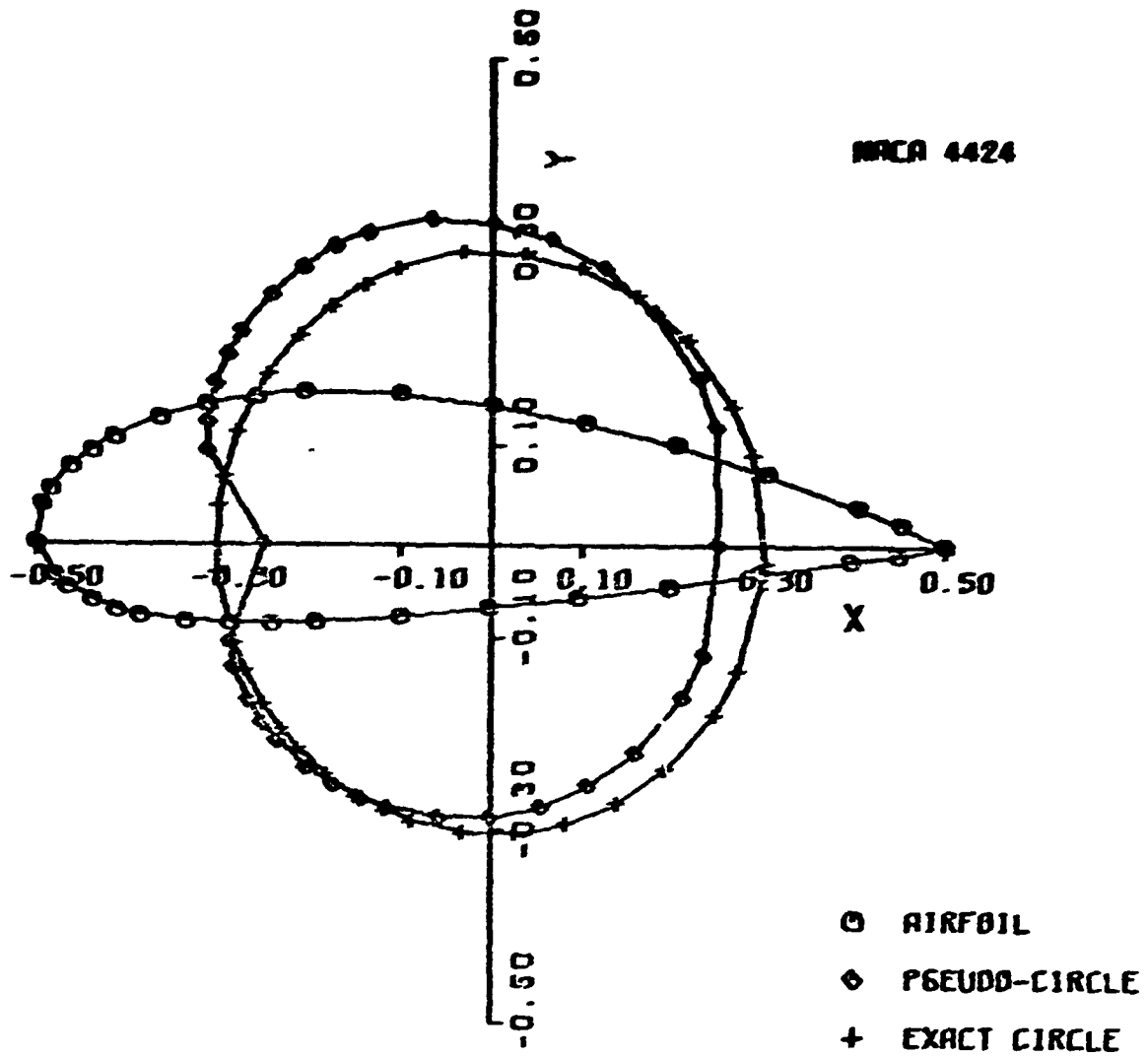


Fig. 3. Transformation of NACA 4424 Airfoil.

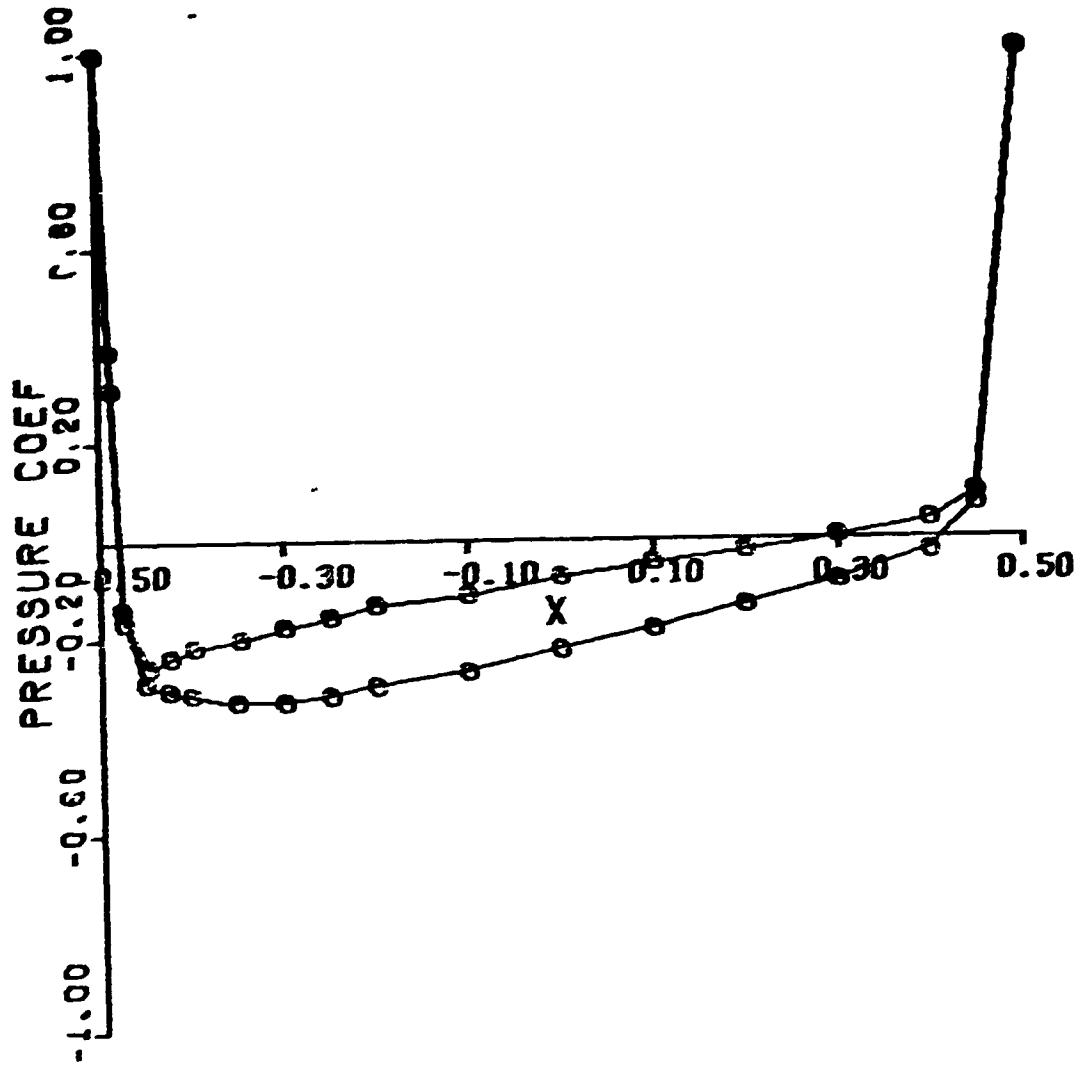


Fig. 4. Pressure Distribution on NACA 1408 Airfoil.

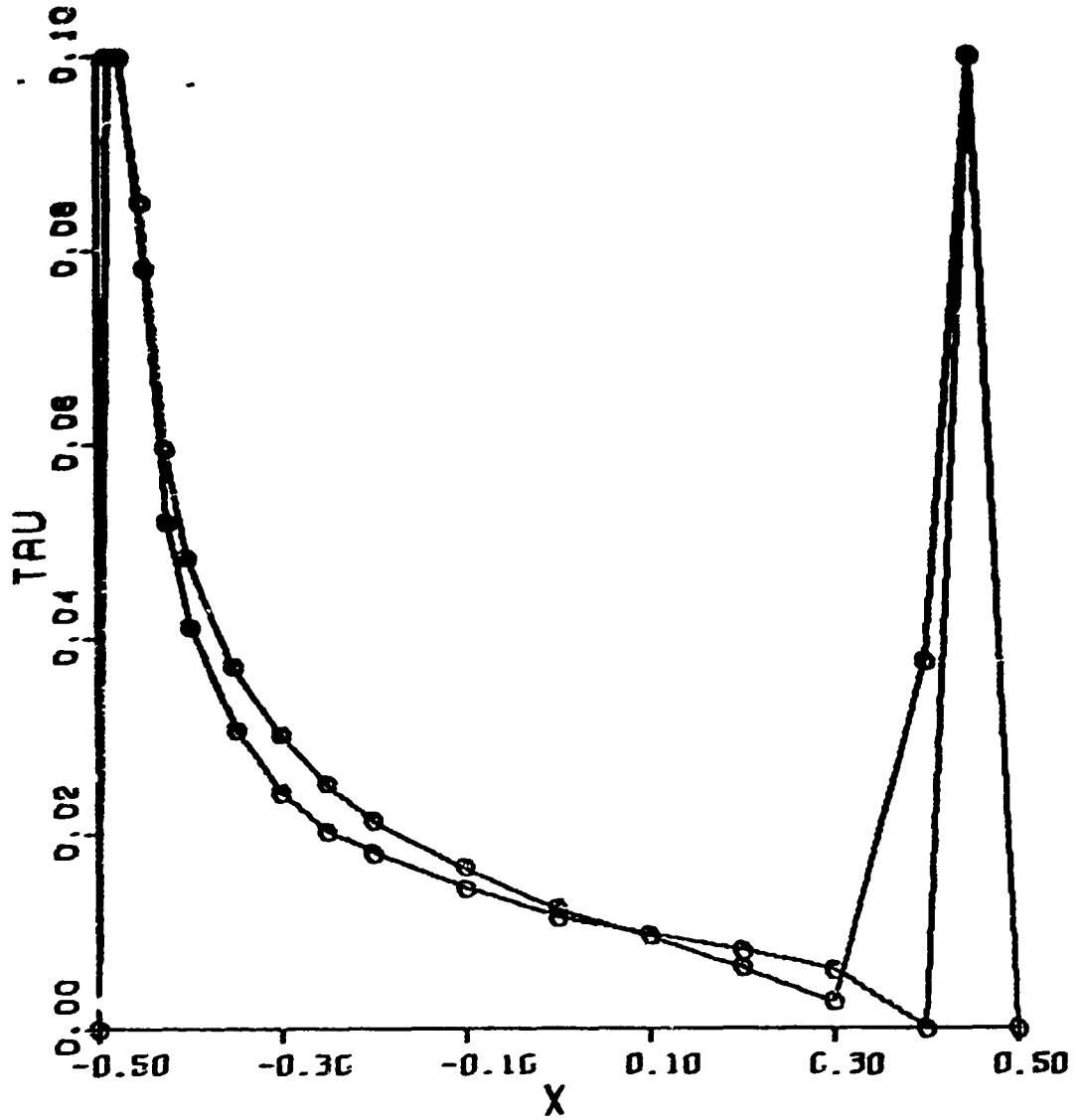


Fig. 5. Shear Stress on NACA 1408 Airfoil.

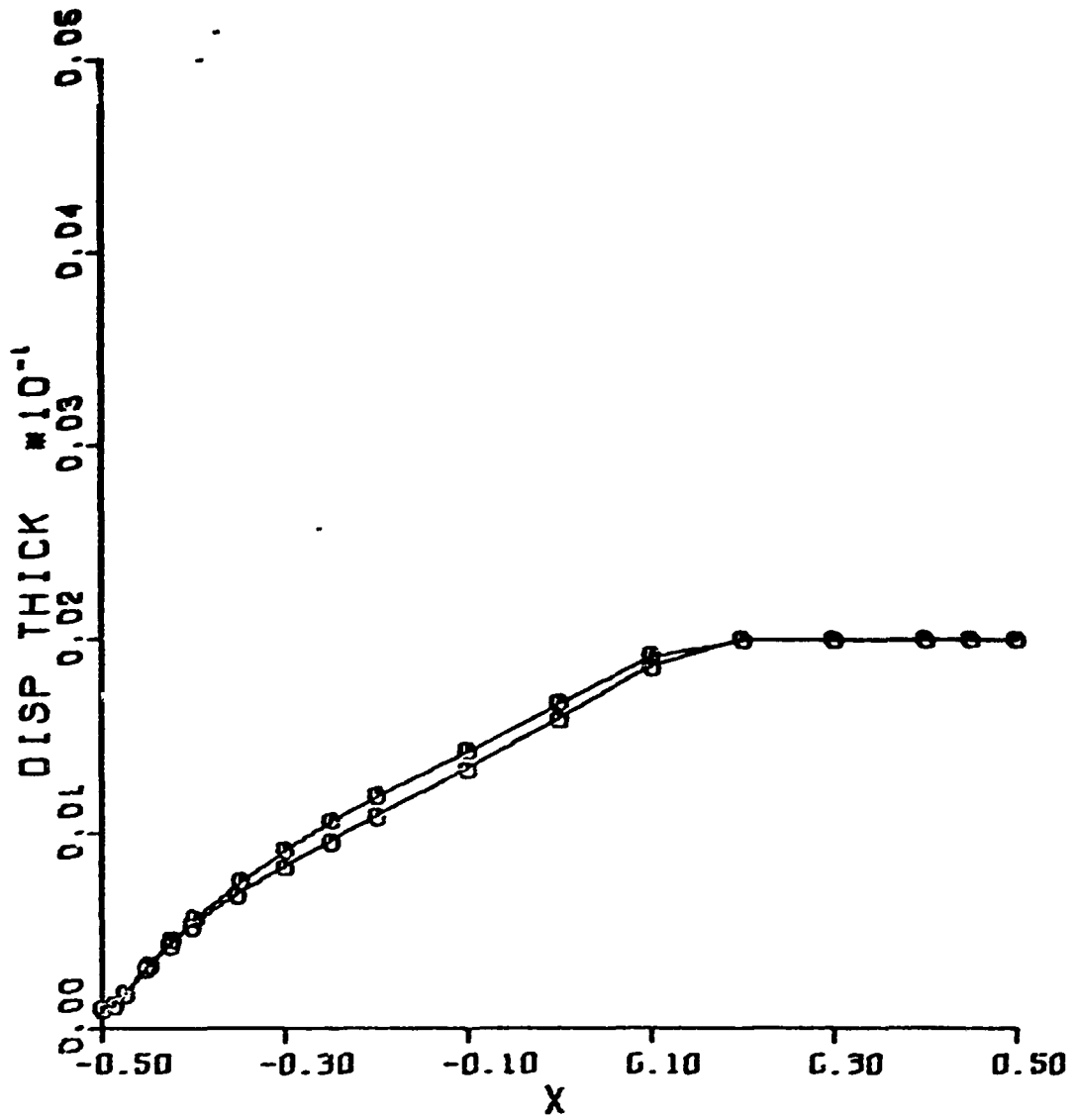


Fig. 6. Boundary Layer Displacement Thickness on NACA 1408 Airfoil.

Boundary Layer Parameters

Pressure coefficients, shear stress, and boundary layer displacement thickness distributions are qualitatively correct (Figs. 4, 5, and 6) upstream of the separation point. As a quantitative check, the separation point for uniform flow around a circle was computed. Subprogram BOUND found this point to be at  $105^\circ$  from the upstream stagnation point. This agrees well with values from  $104.5^\circ$  to  $108.8^\circ$  determined by various investigators, as cited by Schlichting.

Running Time and Core Memory Required

Computer time required for program MAGIC is a function of airfoil shape, number of points, and accuracy required. The NACA 1408 airfoil, with 34 points defined, required approximately 50 seconds of CDC-6600 central processor time and two iterations to obtain a displacement thickness accuracy of .1% of chord length.

Approximately 40,000 octal words of core memory were required.

## VI. Conclusions and Recommendations

### Conclusions

Based upon the results shown in the preceding chapter, the following conclusions were drawn from this study:

1. Theodorsen's method computes values of zero lift angle of attack and potential flow surface velocities very accurately.

2. The Karman-Pohlhausen method of solving the boundary layer equations yields good results upstream of the separation point. No useful information is obtained from these equations downstream of the separation point. Knowledge of the shape factor permits determination of the coefficients in the assumed velocity profile at any point along the surface.

3. Program MAGIC is a practical means of analyzing incompressible flow about an airfoil, without resort to small perturbation or inviscid assumptions. Core memory and central processor requirements are very reasonable for an analysis of this magnitude. Input data requirements are minimal.

### Recommendations

The following recommendations are made for future studies in extension of this one:

1. Program BOUND could be modified to permit boundary layer computations when angle of attack is not zero.

2. Integration of pressure distribution and shear stress would provide drag, moment, and center of pressure information.

3. According to Giesing (Ref 2), Theodorsen's method can be extended to linear arrangements of identical airfoils. Program MAGIC, so extended, could be of considerable value in cascade theory.

4. Theodorsen states that accounting for leading edge and trailing edge radii in locating the coordinate system origin improves the rate of convergence of the iteration on  $\epsilon$ . Inclusion of this correction might result in some saving in computer time.

5. Numerical derivatives of a higher order of accuracy near the leading edge would probably improve velocities computed in that region.

6. The inverse problem (see Ref 4) could be programmed. That is, given a desired pressure distribution, the required airfoil shape could be determined.

7. A more graphic means of input and output could be obtained by adapting the program to the cathode ray tube display terminal.

Bibliography

1. Abbott, Ira H. and Albert E. von Doenhoff. Theory of Wing Sections. New York: McGraw-Hill Book Co., 1949.
2. Giesing, Joseph P. Potential Flow About Two-Dimensional Airfoils. Report No. LB31946. McDonnell-Douglas Aircraft Company, 1 December 1965 (Revised 10 May 1968).
3. Schlichting, H. Boundary Layer Theory (Sixth Edition). New York: McGraw-Hill Book Co., 1968.
4. Theodorsen, T. and I. E. Garrick. General Potential Theory of Arbitrary Wing Sections. NACA Report No. 452. Washington: National Advisory Committee for Aeronautics, 1933.

Appendix A

Computer Program and Sample Output Format

Reproduced from  
best available copy.

XX  
 XX  
 XX

PROGRAM MAGIC (INPUT, OUTPUT, PARAMETER, TABLE OUTPUT, PLOT)  
 MAGIC IS A GENERALIZED PROGRAM FOR ANALYSIS OF STEADY VISCOUS INCOMPRESSIBLE,  
 TWO-DIMENSIONAL FLOW AROUND AN AIRFOIL OF ARBITRARY SHAPE. IT UTILIZES  
 THE ORTHOGONAL MESH AND THE MURMAN-FORMLAN-TRN METHOD. OUTPUTS ARE DESCRIBED  
 BY SUBROUTINE TRO AND ROUTE.

MAGIC DEFINES THE FOLLOWING INPUTS (FORBAT):  
 A - DESIGNATION OF AIRFOIL (AIC)  
 B - NUMBER OF POINTS (N)  
 C - X AND Y FOR EACH POINT (XIP, YI)  
 D - PLACING TURBULENCE  
 E - ANGLE OF ATTACK (ALPHA)  
 F - REYNOLDS NUMBER (RE)  
 G - THE NUMBER OF POINTS IS LIMITED TO 47. SEE SUBROUTINE TRO FOR ADDITIONAL  
 INPUT DATA SPECIFICATIONS.

MAGIC PRINTS APPROXIMATELY 40,000 POINTS OF CURVE LENGTH, NUMBER OF POINTS, AND ACCURACY  
 REQUIREMENTS.

OPERATION OF MAGICAL OUTPUT VARIABLES:-  
 C - ARRAY C GIVES HIGH-TO-LOW ORDER COEFFICIENTS OF SIXTH-ORDER POLYNOMIAL.  
 C - ARRAY D GIVES HIGH-TO-LOW ORDER COEFFICIENTS OF SIXTH-ORDER POLYNOMIAL.  
 C - C1 IS DISPLACEMENT INTEGRAL.  
 C - C2 IS MOMENTUM INTEGRAL.  
 C - C3 IS SHEAR STRESS AT THE AIRFOIL SURFACE.  
 C - C4 IS THE SWEEP FACTOR.  
 C - (XN, YN), AND (XN, YN) ARE CARTESIAN COORDINATES IN THE THREE  
 TRANSFORMATION PLANES.  
 C - (XN, YN) AND (XN, YN) ARE RADIAL COORDINATES IN THE RECIRCULATING  
 AND EXACT CIRCLE PLANES.  
 C - PSI IS THE MAGNIFICATION FACTOR IN THE RECIRCULATING PLANE.  
 C - PSI IS THE MAGNIFICATION FACTOR IN THE EXACT CIRCLE PLANE.  
 C - VTI IS THE SURFACE VELOCITY/MAGNIFICATION VELOCITY RATIO.  
 C - CR IS THE PRESSURE COEFFICIENT.  
 C - EPS IS (OMEGA-TM/TAU).  
 C - ALPHA IS THE ANGLE OF ATTACK.

- 47 -

C DATA IS THE ZERO LEFT BRANCH OF ATTACK.

```

60 C
61 C
62 C
63 C
64 C
65 C
66 C
67 C
68 C
69 C
70 C
71 C
72 C
73 C
74 C
75 C
76 C
77 C
78 C
79 C
80 C
81 C
82 C
83 C
84 C
85 C
86 C
87 C
88 C
89 C
90 C
91 C
92 C
93 C
94 C
95 C
96 C
97 C
98 C
99 C
100 C
101 C
102 C
103 C
104 C
105 C
106 C
107 C
108 C
109 C
110 C
111 C
112 C
113 C
114 C
115 C
116 C
117 C
118 C
119 C
120 C
121 C
122 C
123 C
124 C
125 C
126 C
127 C
128 C
129 C
130 C
131 C
132 C
133 C
134 C
135 C
136 C
137 C
138 C
139 C
140 C
141 C
142 C
143 C
144 C
145 C
146 C
147 C
148 C
149 C
150 C
151 C
152 C
153 C
154 C
155 C
156 C
157 C
158 C
159 C
160 C
161 C
162 C
163 C
164 C
165 C
166 C
167 C
168 C
169 C
170 C
171 C
172 C
173 C
174 C
175 C
176 C
177 C
178 C
179 C
180 C
181 C
182 C
183 C
184 C
185 C
186 C
187 C
188 C
189 C
190 C
191 C
192 C
193 C
194 C
195 C
196 C
197 C
198 C
199 C
200 C
201 C
202 C
203 C
204 C
205 C
206 C
207 C
208 C
209 C
210 C
211 C
212 C
213 C
214 C
215 C
216 C
217 C
218 C
219 C
220 C
221 C
222 C
223 C
224 C
225 C
226 C
227 C
228 C
229 C
230 C
231 C
232 C
233 C
234 C
235 C
236 C
237 C
238 C
239 C
240 C
241 C
242 C
243 C
244 C
245 C
246 C
247 C
248 C
249 C
250 C
251 C
252 C
253 C
254 C
255 C
256 C
257 C
258 C
259 C
260 C
261 C
262 C
263 C
264 C
265 C
266 C
267 C
268 C
269 C
270 C
271 C
272 C
273 C
274 C
275 C
276 C
277 C
278 C
279 C
280 C
281 C
282 C
283 C
284 C
285 C
286 C
287 C
288 C
289 C
290 C
291 C
292 C
293 C
294 C
295 C
296 C
297 C
298 C
299 C
300 C
301 C
302 C
303 C
304 C
305 C
306 C
307 C
308 C
309 C
310 C
311 C
312 C
313 C
314 C
315 C
316 C
317 C
318 C
319 C
320 C
321 C
322 C
323 C
324 C
325 C
326 C
327 C
328 C
329 C
330 C
331 C
332 C
333 C
334 C
335 C
336 C
337 C
338 C
339 C
340 C
341 C
342 C
343 C
344 C
345 C
346 C
347 C
348 C
349 C
350 C
351 C
352 C
353 C
354 C
355 C
356 C
357 C
358 C
359 C
360 C
361 C
362 C
363 C
364 C
365 C
366 C
367 C
368 C
369 C
370 C
371 C
372 C
373 C
374 C
375 C
376 C
377 C
378 C
379 C
380 C
381 C
382 C
383 C
384 C
385 C
386 C
387 C
388 C
389 C
390 C
391 C
392 C
393 C
394 C
395 C
396 C
397 C
398 C
399 C
400 C
401 C
402 C
403 C
404 C
405 C
406 C
407 C
408 C
409 C
410 C
411 C
412 C
413 C
414 C
415 C
416 C
417 C
418 C
419 C
420 C
421 C
422 C
423 C
424 C
425 C
426 C
427 C
428 C
429 C
430 C
431 C
432 C
433 C
434 C
435 C
436 C
437 C
438 C
439 C
440 C
441 C
442 C
443 C
444 C
445 C
446 C
447 C
448 C
449 C
450 C
451 C
452 C
453 C
454 C
455 C
456 C
457 C
458 C
459 C
460 C
461 C
462 C
463 C
464 C
465 C
466 C
467 C
468 C
469 C
470 C
471 C
472 C
473 C
474 C
475 C
476 C
477 C
478 C
479 C
480 C
481 C
482 C
483 C
484 C
485 C
486 C
487 C
488 C
489 C
490 C
491 C
492 C
493 C
494 C
495 C
496 C
497 C
498 C
499 C
500 C
501 C
502 C
503 C
504 C
505 C
506 C
507 C
508 C
509 C
510 C
511 C
512 C
513 C
514 C
515 C
516 C
517 C
518 C
519 C
520 C
521 C
522 C
523 C
524 C
525 C
526 C
527 C
528 C
529 C
530 C
531 C
532 C
533 C
534 C
535 C
536 C
537 C
538 C
539 C
540 C
541 C
542 C
543 C
544 C
545 C
546 C
547 C
548 C
549 C
550 C
551 C
552 C
553 C
554 C
555 C
556 C
557 C
558 C
559 C
560 C
561 C
562 C
563 C
564 C
565 C
566 C
567 C
568 C
569 C
570 C
571 C
572 C
573 C
574 C
575 C
576 C
577 C
578 C
579 C
580 C
581 C
582 C
583 C
584 C
585 C
586 C
587 C
588 C
589 C
590 C
591 C
592 C
593 C
594 C
595 C
596 C
597 C
598 C
599 C
600 C
601 C
602 C
603 C
604 C
605 C
606 C
607 C
608 C
609 C
610 C
611 C
612 C
613 C
614 C
615 C
616 C
617 C
618 C
619 C
620 C
621 C
622 C
623 C
624 C
625 C
626 C
627 C
628 C
629 C
630 C
631 C
632 C
633 C
634 C
635 C
636 C
637 C
638 C
639 C
640 C
641 C
642 C
643 C
644 C
645 C
646 C
647 C
648 C
649 C
650 C
651 C
652 C
653 C
654 C
655 C
656 C
657 C
658 C
659 C
660 C
661 C
662 C
663 C
664 C
665 C
666 C
667 C
668 C
669 C
670 C
671 C
672 C
673 C
674 C
675 C
676 C
677 C
678 C
679 C
680 C
681 C
682 C
683 C
684 C
685 C
686 C
687 C
688 C
689 C
690 C
691 C
692 C
693 C
694 C
695 C
696 C
697 C
698 C
699 C
700 C
701 C
702 C
703 C
704 C
705 C
706 C
707 C
708 C
709 C
710 C
711 C
712 C
713 C
714 C
715 C
716 C
717 C
718 C
719 C
720 C
721 C
722 C
723 C
724 C
725 C
726 C
727 C
728 C
729 C
730 C
731 C
732 C
733 C
734 C
735 C
736 C
737 C
738 C
739 C
740 C
741 C
742 C
743 C
744 C
745 C
746 C
747 C
748 C
749 C
750 C
751 C
752 C
753 C
754 C
755 C
756 C
757 C
758 C
759 C
760 C
761 C
762 C
763 C
764 C
765 C
766 C
767 C
768 C
769 C
770 C
771 C
772 C
773 C
774 C
775 C
776 C
777 C
778 C
779 C
780 C
781 C
782 C
783 C
784 C
785 C
786 C
787 C
788 C
789 C
790 C
791 C
792 C
793 C
794 C
795 C
796 C
797 C
798 C
799 C
800 C
801 C
802 C
803 C
804 C
805 C
806 C
807 C
808 C
809 C
810 C
811 C
812 C
813 C
814 C
815 C
816 C
817 C
818 C
819 C
820 C
821 C
822 C
823 C
824 C
825 C
826 C
827 C
828 C
829 C
830 C
831 C
832 C
833 C
834 C
835 C
836 C
837 C
838 C
839 C
840 C
841 C
842 C
843 C
844 C
845 C
846 C
847 C
848 C
849 C
850 C
851 C
852 C
853 C
854 C
855 C
856 C
857 C
858 C
859 C
860 C
861 C
862 C
863 C
864 C
865 C
866 C
867 C
868 C
869 C
870 C
871 C
872 C
873 C
874 C
875 C
876 C
877 C
878 C
879 C
880 C
881 C
882 C
883 C
884 C
885 C
886 C
887 C
888 C
889 C
890 C
891 C
892 C
893 C
894 C
895 C
896 C
897 C
898 C
899 C
900 C
901 C
902 C
903 C
904 C
905 C
906 C
907 C
908 C
909 C
910 C
911 C
912 C
913 C
914 C
915 C
916 C
917 C
918 C
919 C
920 C
921 C
922 C
923 C
924 C
925 C
926 C
927 C
928 C
929 C
930 C
931 C
932 C
933 C
934 C
935 C
936 C
937 C
938 C
939 C
940 C
941 C
942 C
943 C
944 C
945 C
946 C
947 C
948 C
949 C
950 C
951 C
952 C
953 C
954 C
955 C
956 C
957 C
958 C
959 C
960 C
961 C
962 C
963 C
964 C
965 C
966 C
967 C
968 C
969 C
970 C
971 C
972 C
973 C
974 C
975 C
976 C
977 C
978 C
979 C
980 C
981 C
982 C
983 C
984 C
985 C
986 C
987 C
988 C
989 C
990 C
991 C
992 C
993 C
994 C
995 C
996 C
997 C
998 C
999 C
1000 C

```

PROGRAM NAME TRACE

```

115  *****
120  *****
125  *****
130  *****
135  *****
140  *****

```

Reproduced from best available copy.

SUBROUTINE TMR3

-----

```

C-----
C     THEN TRANFORMS AN ARBITRARY AIRCRAFT SHAPE FIRST INTO A RECTANGLE
C     THEN INTO AN ELLIPSE. THE AIRCRAFT SHAPE LIST IS ASSUMED TO BE ON
C     THE X-Y PLANE WITH THE TAILING EDGE IN THE X-DIRECTION AND THE FRONT
C     EDGE AT THE ORIGIN. POINTS DEFINING THE AIRCRAFT SURFACE MUST BE IN
C     ORDER OF INCREASING X AND CONTINUED IN THE COUNTERCLOCKWISE DIRECTION. ALL
C     COORDINATE MUST BE REFERENCED TO A UNIT CHORD LENGTH.

```

```

C-----
C     THEN COMPUTES THE FOLLOWING INPUT

```

```

C     POSITIONING OF AIRCRAFT
C     X-ORIGIN OF AIRCRAFT
C     Y-ORIGIN OF AIRCRAFT
C     AIRCRAFT LENGTH
C     AIRCRAFT WIDTH
C     AIRCRAFT AREA
C     AIRCRAFT PERIMETER
C     AIRCRAFT CHORD
C     AIRCRAFT AREA
C     AIRCRAFT PERIMETER

```

```

C-----
C     THEN COMPUTES THE COEFFICIENTS IN ALL THREE PLANES, ALSO COEFFICIENTS IN
C     THE X-Y PLANE AND THE X-Z PLANE. ALSO COMPUTES THE QUANTITIES USED
C     TO COMPUTE THE CORRECTIONS TO THE AIRCRAFT SURFACE AREA AND
C     AIRCRAFT PERIMETER. ALSO COMPUTES THE CORRECTIONS TO THE AIRCRAFT
C     SURFACE AREA AND PERIMETER.

```

```

C-----
C     THEN COMPUTES THE CORRECTIONS TO THE AIRCRAFT SURFACE AREA AND
C     PERIMETER. ALSO COMPUTES THE CORRECTIONS TO THE AIRCRAFT SURFACE
C     AREA AND PERIMETER.

```

```

C-----
C     THEN COMPUTES THE CORRECTIONS TO THE AIRCRAFT SURFACE AREA AND
C     PERIMETER. ALSO COMPUTES THE CORRECTIONS TO THE AIRCRAFT SURFACE
C     AREA AND PERIMETER.

```

```

C-----
C     THEN COMPUTES THE CORRECTIONS TO THE AIRCRAFT SURFACE AREA AND
C     PERIMETER. ALSO COMPUTES THE CORRECTIONS TO THE AIRCRAFT SURFACE
C     AREA AND PERIMETER.

```

```

C-----
C     THEN COMPUTES THE CORRECTIONS TO THE AIRCRAFT SURFACE AREA AND
C     PERIMETER. ALSO COMPUTES THE CORRECTIONS TO THE AIRCRAFT SURFACE
C     AREA AND PERIMETER.

```

```

C-----
C     THEN COMPUTES THE CORRECTIONS TO THE AIRCRAFT SURFACE AREA AND
C     PERIMETER. ALSO COMPUTES THE CORRECTIONS TO THE AIRCRAFT SURFACE
C     AREA AND PERIMETER.

```

```

C-----
C     THEN COMPUTES THE CORRECTIONS TO THE AIRCRAFT SURFACE AREA AND
C     PERIMETER. ALSO COMPUTES THE CORRECTIONS TO THE AIRCRAFT SURFACE
C     AREA AND PERIMETER.

```

SUSPECTIVE TRM TRM

67 AUGUST 11 1993  
 68 AUGUST 12 1993  
 69 AUGUST 13 1993  
 70 AUGUST 14 1993  
 71 AUGUST 15 1993  
 72 AUGUST 16 1993  
 73 AUGUST 17 1993  
 74 AUGUST 18 1993  
 75 AUGUST 19 1993  
 76 AUGUST 20 1993  
 77 AUGUST 21 1993  
 78 AUGUST 22 1993  
 79 AUGUST 23 1993  
 80 AUGUST 24 1993  
 81 AUGUST 25 1993  
 82 AUGUST 26 1993  
 83 AUGUST 27 1993  
 84 AUGUST 28 1993  
 85 AUGUST 29 1993  
 86 AUGUST 30 1993  
 87 AUGUST 31 1993  
 88 AUGUST 31 1993  
 89 AUGUST 31 1993  
 90 AUGUST 31 1993  
 91 AUGUST 31 1993  
 92 AUGUST 31 1993  
 93 AUGUST 31 1993  
 94 AUGUST 31 1993  
 95 AUGUST 31 1993  
 96 AUGUST 31 1993  
 97 AUGUST 31 1993  
 98 AUGUST 31 1993  
 99 AUGUST 31 1993  
 100 AUGUST 31 1993  
 101 AUGUST 31 1993  
 102 AUGUST 31 1993  
 103 AUGUST 31 1993  
 104 AUGUST 31 1993  
 105 AUGUST 31 1993  
 106 AUGUST 31 1993  
 107 AUGUST 31 1993  
 108 AUGUST 31 1993  
 109 AUGUST 31 1993  
 110 AUGUST 31 1993





CDC 6000 PFM V3.0-0010 OPT01 11/04/71 15.00.00. PAGE 9  
 Y=30.9.90.0

225	SUBROUTINE TRANZ CALL ARTS10.0.0.0.0.0.0.0.0.0 CALL LINFRXV.0.0.0.0.0.0.0.0.0.0 CALL SYMPL.0.0.0.0.0.0.0.0.0.0 CALL PLOT10.0.0.0.0.0.0.0.0.0.0 001 CONTINUE C PLOT PRESSURE COEFFICIENT XIN=10.0 XIN=21.0 CPIN=10.0 CPIN=21.0 CALL PLOT10.0.0.0.0.0.0.0.0.0.0 CALL ARTS10.0.0.0.0.0.0.0.0.0.0 CALL ARTS10.0.0.0.0.0.0.0.0.0.0 CALL LEAF10.0.0.0.0.0.0.0.0.0.0 PFD
270	
233	

```

C SUBROUTINE PMPVAL (N,PI)
C PMPVAL OFFICES THE INTERGRANDS MPPTS IN COMPUTING PHE AND CPE, AND SECURES
C FUNCTION AIMS, AS WELL AS LIBRARY FUNCTION.
C
C COMMON/ALCK/INT,PI,INT,C(10),D(10),T,CTA(10),CPS(100),PPT(100)
C PRINT*,'11'
C FROM PHE INTERGRAND
C 11 PHE(1)PHE(2)PHE(3)PHE(4)PHE(5)PHE(6)PHE(7)PHE(8)PHE(9)PHE(10)/10.000
C 12 TP 12
C FROM PHE INTERGRAND
C 13 ZCATN(PI)PHE,PSC,H,PI,PI,PI
C 14 C(10),D(10),T,CTA(10),CPS(100),PPT(100)
C 15 WATN(CPE),PHE,PPT(100)
C 16 PRINT*,'12.000'
C 17 RETURN
C PHE

```

Reproduced from  
Last available copy.

9 SUBROUTINE ROUND TRACE  
 10 SUBROUTINE ROUND  
 15 COMPUTE BOUNDARY LAYER PARAMETERS FOR AN ARBITRARY AIRFOIL  
 16 SHAPE IMPERSON IN LAMINAR INCOMPRESSIBLE FLOW. THE KARMAN-POLLHAUSEN  
 17 METHOD IS USED.  
 18 ROUND REQUIRES THE FOLLOWING INPUT  
 19 NUMBER OF POINTS  
 20 X AND Y FOR EACH POINT  
 21 TANGENTIAL PERPENDICULAR VELOCITY RATIO FOR EACH POINT  
 22 VISCOSITY  
 23 DENSITY  
 24 FREE-STREAM VELOCITY  
 25 ROUND OUTPUTS SURFACE STRESS AT SURFACE AND MOMENTUM AND DISPLACEMENT  
 26 BOUNDARY LAYER THICKNESSES, AS WELL AS VARIOUS QUANTITIES USED IN  
 27 THESE COMPUTATIONS.  
 28 ROUND USES FUNCTION ATN IN CONNECTION TO LIBRARY SUBROUTINES AND FUNCTIONS.  
 29 DIMENSION Z(100), X(100), Y(100), V(100), P(100), F(100), LAMDA(100),  
 30 X1(100), Y1(100), X2(100), Y2(100), X3(100), Y3(100), X4(100), Y4(100),  
 31 X5(100), Y5(100), X6(100), Y6(100), X7(100), Y7(100), X8(100), Y8(100),  
 32 X9(100), Y9(100), X10(100), Y10(100), X11(100), Y11(100), X12(100), Y12(100),  
 33 X13(100), Y13(100), X14(100), Y14(100), X15(100), Y15(100), X16(100), Y16(100),  
 34 X17(100), Y17(100), X18(100), Y18(100), X19(100), Y19(100), X20(100), Y20(100),  
 35 X21(100), Y21(100), X22(100), Y22(100), X23(100), Y23(100), X24(100), Y24(100),  
 36 X25(100), Y25(100), X26(100), Y26(100), X27(100), Y27(100), X28(100), Y28(100),  
 37 X29(100), Y29(100), X30(100), Y30(100), X31(100), Y31(100), X32(100), Y32(100),  
 38 X33(100), Y33(100), X34(100), Y34(100), X35(100), Y35(100), X36(100), Y36(100),  
 39 X37(100), Y37(100), X38(100), Y38(100), X39(100), Y39(100), X40(100), Y40(100),  
 40 X41(100), Y41(100), X42(100), Y42(100), X43(100), Y43(100), X44(100), Y44(100),  
 41 X45(100), Y45(100), X46(100), Y46(100), X47(100), Y47(100), X48(100), Y48(100),  
 42 X49(100), Y49(100), X50(100), Y50(100), X51(100), Y51(100), X52(100), Y52(100),  
 43 X53(100), Y53(100), X54(100), Y54(100), X55(100), Y55(100), X56(100), Y56(100),  
 44 X57(100), Y57(100), X58(100), Y58(100), X59(100), Y59(100), X60(100), Y60(100),  
 45 X61(100), Y61(100), X62(100), Y62(100), X63(100), Y63(100), X64(100), Y64(100),  
 46 X65(100), Y65(100), X66(100), Y66(100), X67(100), Y67(100), X68(100), Y68(100),  
 47 X69(100), Y69(100), X70(100), Y70(100), X71(100), Y71(100), X72(100), Y72(100),  
 48 X73(100), Y73(100), X74(100), Y74(100), X75(100), Y75(100), X76(100), Y76(100),  
 49 X77(100), Y77(100), X78(100), Y78(100), X79(100), Y79(100), X80(100), Y80(100),  
 50 X81(100), Y81(100), X82(100), Y82(100), X83(100), Y83(100), X84(100), Y84(100),  
 51 X85(100), Y85(100), X86(100), Y86(100), X87(100), Y87(100), X88(100), Y88(100),  
 52 X89(100), Y89(100), X90(100), Y90(100), X91(100), Y91(100), X92(100), Y92(100),  
 53 X93(100), Y93(100), X94(100), Y94(100), X95(100), Y95(100), X96(100), Y96(100),  
 54 X97(100), Y97(100), X98(100), Y98(100), X99(100), Y99(100), X100(100), Y100(100)  
 55 COMPUTE POLAR COORDINATES OF EACH POINT AND FIND LEADING EDGE

```

SUBROUTINE MOUNTM  TRACE
50  DO 1001 I=1,N
    00011)SORT(X(I),Z(I),Y(I),E=2)
    77)ATT=ACIN(V(I),RAD(I))
    78)Y(I),FO=Z(I) L=Z(I)
1001 CONTINUE
C COMPUTE APP LENGTHS
    ACC=Z(I)
    DO 1002 I=5,N
1002 A=Z(I)*COS(SIN(SIN(I)*COS(RA(I)-1)*COS(1)*RAD(I)+1)*COS(7E1A(
    171)*2*PI*(I-1)))
C COMPUTE STREAMWISE COEFFICIENT OF EACH POINT
C
    LEMPLE=1
    VEL=Z(I)
    TEL=Z(I)
1003 SORT(X(I),Z(I),Y(I),E=1)
    77)ATT=ACIN(V(I),RAD(I))
    78)Y(I),FO=Z(I) L=Z(I)
    GO TO 1007
1010 CONTINUE
    L=Z(I)+1
    DO 1004 I=L,N
1004 X(I)=Z(I)+1)*ADP(I)
C COMPUTE VELOCITY DISTRIBUTURE ON UPPER SURFACE
C
    WTV(L)=(-2.*WTV(L)+4.*WTV(L-1)-WTV(L-2))/*(L-2)
    WTV(3)=(WTV(2)-4.*WTV(1)+3.*WTV(0))/(5(3)-4(1))
    TEL=1
1005 WTV(I)=(WTV(I)+WTV(I-1)+WTV(I-2))/(5(I)-4(I+1))
    I=I-1
    GO TO 1007
1011 CONTINUE
    WTV(L)=(777/WTV(L))
    WTV(L)=(-.652+WTV)/C(WTV(L))**2
    TEL=1
1012 Z(I)=Z(I)+Z(I)*Z(I)*C(I)-S(I+1)
    WTV(I)=WTV(I)+WTV(I)
    FF(I)=ATTW(I)*.764*W(I)
    Z(I)=Z(I)+FF(I)/WTV(I)
    FF(I)=ATTW(I)*.764*W(I)
    WTV(I)=ATTW(I)*.764*W(I)
    FF(I)=ATTW(I)*.764*W(I)
1016 L=Z(I)+ATTW(I)*.764*W(I)
    WTV(I)=ATTW(I)*.764*W(I)
    I=I-1
    GO TO 1012
1017 CONTINUE

```

-57-



SUBROUTINE "CUND TRACE

```

1022 WRITE(C,1000)
      FORMAT('C', 'CUND SUBROUTINE')
      NO 1024 CALL N
1029 WRITE(C,1000) I, J, K, L, M, N, O, P, Q, R, S, T, U, V, W, X, Y, Z, AA, AB, AC, AD, AE, AF, AG, AH, AI, AJ, AK, AL, AM, AN, AO, AP, AQ, AR, AS, AT, AU, AV, AW, AX, AY, AZ, BA, BB, BC, BD, BE, BF, BG, BH, BI, BJ, BK, BL, BM, BN, BO, BP, BQ, BR, BS, BT, BU, BV, BW, BX, BY, BZ, CA, CB, CC, CD, CE, CF, CG, CH, CI, CJ, CK, CL, CM, CN, CO, CP, CQ, CR, CS, CT, CU, CV, CW, CX, CY, CZ, DA, DB, DC, DD, DE, DF, DG, DH, DI, DJ, DK, DL, DM, DN, DO, DP, DQ, DR, DS, DT, DU, DV, DW, DX, DY, DZ, EA, EB, EC, ED, EE, EF, EG, EH, EI, EJ, EK, EL, EM, EN, EO, EP, EQ, ER, ES, ET, EU, EV, EW, EX, EY, EZ, FA, FB, FC, FD, FE, FF, FG, FH, FI, FJ, FK, FL, FM, FN, FO, FP, FQ, FR, FS, FT, FU, FV, FW, FX, FY, FZ, GA, GB, GC, GD, GE, GF, GG, GH, GI, GJ, GK, GL, GM, GN, GO, GP, GQ, GR, GS, GT, GU, GV, GW, GX, GY, GZ, HA, HB, HC, HD, HE, HF, HG, HH, HI, HJ, HK, HL, HM, HN, HO, HP, HQ, HR, HS, HT, HU, HV, HW, HX, HY, HZ, IA, IB, IC, ID, IE, IF, IG, IH, II, IJ, IK, IL, IM, IN, IO, IP, IQ, IR, IS, IT, IU, IV, IW, IX, IY, IZ, JA, JB, JC, JD, JE, JF, JG, JH, JI, JJ, JK, JL, JM, JN, JO, JP, JQ, JR, JS, JT, JU, JV, JW, JX, JY, JZ, KA, KB, KC, KD, KE, KF, KG, KH, KI, KJ, KK, KL, KM, KN, KO, KP, KQ, KR, KS, KT, KU, KV, KW, KX, KY, KZ, LA, LB, LC, LD, LE, LF, LG, LH, LI, LJ, LK, LL, LM, LN, LO, LP, LQ, LR, LS, LT, LU, LV, LW, LX, LY, LZ, MA, MB, MC, MD, ME, MF, MG, MH, MI, MJ, MK, ML, MM, MN, MO, MP, MQ, MR, MS, MT, MU, MV, MW, MX, MY, MZ, NA, NB, NC, ND, NE, NF, NG, NH, NI, NJ, NK, NL, NM, NO, NP, NQ, NR, NS, NT, NU, NV, NW, NX, NY, NZ, OA, OB, OC, OD, OE, OF, OG, OH, OI, OJ, OK, OL, OM, ON, OO, OP, OQ, OR, OS, OT, OU, OV, OW, OX, OY, OZ, PA, PB, PC, PD, PE, PF, PG, PH, PI, PJ, PK, PL, PM, PN, PO, PP, PQ, PR, PS, PT, PU, PV, PW, PX, PY, PZ, QA, QB, QC, QD, QE, QF, QG, QH, QI, QJ, QK, QL, QM, QN, QO, QP, QQ, QR, QS, QT, QU, QV, QW, QX, QY, QZ, RA, RB, RC, RD, RE, RF, RG, RH, RI, RJ, RK, RL, RM, RN, RO, RP, RQ, RR, RS, RT, RU, RV, RW, RX, RY, RZ, SA, SB, SC, SD, SE, SF, SG, SH, SI, SJ, SK, SL, SM, SN, SO, SP, SQ, SR, SS, ST, SU, SV, SW, SX, SY, SZ, TA, TB, TC, TD, TE, TF, TG, TH, TI, TJ, TK, TL, TM, TN, TO, TP, TQ, TR, TS, TT, TU, TV, TW, TX, TY, TZ, UA, UB, UC, UD, UE, UF, UG, UH, UI, UJ, UK, UL, UM, UN, UO, UP, UQ, UR, US, UT, UY, UV, UW, UX, UY, UZ, VA, VB, VC, VD, VE, VF, VG, VH, VI, VJ, VK, VL, VM, VN, VO, VP, VQ, VR, VS, VT, VU, VV, VW, VX, VY, VZ, WA, WB, WC, WD, WE, WF, WG, WH, WI, WJ, WK, WL, WM, WN, WO, WP, WQ, WR, WS, WT, WU, WV, WW, WX, WY, WZ, XA, XB, XC, XD, XE, XF, XG, XH, XI, XJ, XK, XL, XM, XN, XO, XP, XQ, XR, XS, XT, XU, XV, XW, XX, XY, XZ, YA, YB, YC, YD, YE, YF, YG, YH, YI, YJ, YK, YL, YM, YN, YO, YP, YQ, YR, YS, YT, YU, YV, YW, YX, YY, YZ, ZA, ZB, ZC, ZD, ZE, ZF, ZG, ZH, ZI, ZJ, ZK, ZL, ZM, ZN, ZO, ZP, ZQ, ZR, ZS, ZT, ZU, ZV, ZW, ZX, ZY, ZZ
1070 CONTINUE
C FLOT SHEAR STRESS
C
      X(1000)=0
      Y(1000)=0
      Z(1000)=0
      TAU(1000)=0
      CALL PLOT(C,1000)
      CALL AXIS(C,1000)
      CALL LINE(C,1000)
      CALL PLOT(C,1000)
1077 CONTINUE
C FLOT DISPLACEMENT THROUGHNESS
C
      X(1000)=0
      Y(1000)=0
      Z(1000)=0
      CALL PLOT(C,1000)
      CALL AXIS(C,1000)
      CALL LINE(C,1000)
      CALL PLOT(C,1000)
1077 CONTINUE

```

Reproduced from  
best available copy.





CDC 6500 PTK V2.C-201A OPT=1 11/05/71 14.09.99.

SUBROUTINE MIXFO YRAC

CALL SYSTEM (207,11)

STOP

1000 FORMAT(1M,12,5M, 1M12,3M,1M) FOR SUPERUTIME PTIME

1001 FORMAT (1M,12,5M,1M,1M) FOR SUPERUTIME PTIME

END

MIXFO11

MIXFO12

MIXFO13

MIXFO14

MIXFO15

Reproduced from  
best available copy. (1)





SUBROUTINE PLSO TRACE

SUPERUTINE PLSOX,Y,N,K,C,LIST,EMX,EPMS,EPFO)

PLSO POLYNOMIAL LEAST SQUARE CURVE FIT

PLSO WILL FIT A GIVEN SET OF DATA TO A POLYNOMIAL OF DEGREE K OF THE FORM...

Y=C(1)\*X^(K-1)+C(2)\*X^(K-2)+...+C(K-1)\*X+C(K)

PLSO THEN COMPUTES THE MAXIMUM ERROR AND ROOT MEAN SQUARE ERROR OBTAINED BY USING THE C COEFFICIENTS TO COMPUTE Y FROM X

WHERE...

DIMENSION X(N), Y(N), C(L)

WHERE L IS K+1

CALL PLSOX(Y,N,K,C,LIST,EMX,EPMS,EPFO)

WHERE...

X IS THE ARRAY OF N INDEPENDENT VARIABLES

Y IS THE ARRAY OF N DEPENDENT VARIABLES

N IS THE NUMBER OF INDEPENDENT VARIABLES

K IS THE DEGREE OF THE LEAST SQUARE POLYNOMIAL

C IS THE ARRAY OF THE COEFFICIENTS, HIGH ORDER TO LOW ORDER, OF THE LEAST SQUARE POLYNOMIAL

LIST=1 SURVEYS THE ERROR ANALYSIS OUTPUT LIST=2 GIVES THE ERROR ANALYSIS OUTPUT

EMX IS THE MAXIMUM ABSOLUTE ERROR OBTAINED BY USING THE COMPUTED C COEFFICIENTS TO APPROXIMATE THE DEPENDENT VARIABLE

EPMS IS THE ROOT MEAN SQUARE ERROR OBTAINED BY USING THE COMPUTED C COEFFICIENTS TO APPROXIMATE THE DEPENDENT VARIABLE

EPFO IS THE MAXIMUM DEVIATION FROM UNITY IN THE LINEAR SYSTEM CHECK SOLUTION

PLSO CALLS SUBROUTINE PLSOX AND MIXED

PLSO USES 1339 CELLS OF PLANK COMMON

COMMON MIXFOT(664), OF, OIF, I, J, JC, JM,

- PLSC0001 PLSC0002 PLSC0003 PLSC0004 PLSC0005 PLSC0006 PLSC0007 PLSC0008 PLSC0009 PLSC0010 PLSC0011 PLSC0012 PLSC0013 PLSC0014 PLSC0015 PLSC0016 PLSC0017 PLSC0018 PLSC0019 PLSC0020 PLSC0021 PLSC0022 PLSC0023 PLSC0024 PLSC0025 PLSC0026 PLSC0027 PLSC0028 PLSC0029 PLSC0030 PLSC0031 PLSC0032 PLSC0033 PLSC0034 PLSC0035 PLSC0036 PLSC0037 PLSC0038 PLSC0039 PLSC0040 PLSC0041 PLSC0042 PLSC0043 PLSC0044 PLSC0045 PLSC0046 PLSC0047 PLSC0048 PLSC0049 PLSC0050 PLSC0051 PLSC0052 PLSC0053 PLSC0054 PLSC0055

165

```

      L, LL, LU, M, SUM, XI, XM(57A),
      XMAX, XMIN, XP, YC, YH(48)
      DIMENSION X(N), Y(N), C(24),
      EQUIVALENCE XOB(40), YOP(24),
      DATE (INTXPT(1),XOP(1)), (PTENT(07),NYEP(1))
      NMAX/ 23/
      C CHECK K AND N FOR RANGE
      C
      C IF (K.GT. NMAX .OR. N.LE. N .OR. M.LE. 0) GO TO 200
      L=K+1
      C FIND MINIMUM AND MAXIMUM VALUES FOR X
      C
      XMIN=X(1)
      XMAX=X(1)
      DO 10 I=2,N
      XMIN=AMIN(XMIN,X(I))
      XMAX=AMAX(XMAX,X(I))
      C TWO POINT DEFINITION SPAYS FOR SUMPING
      C
      MZ=200+1
      DO 20 I=1,M
      XOP(I)=C+0
      DO 20 J=1,L
      XOP(I)=3.0
      C
      C DETERMINE RANGE OF Y TO (-1.0) AND
      C COMPUTE SUMS OF SQUARES OF X AND CLMC
      C OF Y TIMES SQUARES OF X
      C
      C1 = 2.0 / (XMAX - XMIN)
      C2 = (YMAX + XMIN) / (XMAX - XMIN)
      LL=0
      LU=200+1
      DO 40 I=1,M
      YI = C1 * X(I) + C2
      YC2(J)=YOP(J)+YI
      YOP(J)=YOP(J)+YI
      XOP(I)=XOP(I)+YI
      DO 40 J=LL,LU
      XOP(I)=YOP(J)+XO
      XOP(I)=XOP(I)+YI
      C
      C TOPE ABOVE COMPUTED SUMS IN ARRAY MP
      C AND COMPUTE POW SUMS FOR CHECK SOLUTION
      DO 50 I=1,L
      LL=70
      Y(LL)=0.0
      LU=(I-1)*L
      JK=I-1

```

PLSO0076  
 PLSO0077  
 PLSO0078  
 PLSO0079  
 PLSO0080  
 PLSO0081  
 PLSO0082  
 PLSO0083  
 PLSO0084  
 PLSO0085  
 PLSO0086  
 PLSO0087  
 PLSO0088  
 PLSO0089  
 PLSO0090  
 PLSO0091  
 PLSO0092  
 PLSO0093  
 PLSO0094  
 PLSO0095  
 PLSO0096  
 PLSO0097  
 PLSO0098  
 PLSO0099  
 PLSO0100  
 PLSO0101  
 PLSO0102  
 PLSO0103  
 PLSO0104  
 PLSO0105  
 PLSO0106  
 PLSO0107  
 PLSO0108  
 PLSO0109  
 PLSO0110  
 PLSO0111

-66-

```

SUBROUTINE PLSO TRACE
    DO 50 J=1,L
    JK=JK+1
    JC=JU+J
    XM(JC)=XDP(JK)
    YM(1L)=YM(1L)+X*W(JC)
    DO 60 I=1,L
    YM(I)=YDPI(I)
    C SOLVE THE SYSTEM XM=C*Y
    C CALL MIXER(XM,YM,AL,P)
    C REORDER AND MOVE SOLUTION TO C AND FIND
    C MAXIMUM ERROR IN CHECK SOLUTION
    EMAX=0.0
    DO 70 I=1,L
    JK=JK+2
    C(JK)=Y(I)
    JREI=L
    EMAX=MAX(EMAX,ABS(Y(I)-X*W(JC)-1.0))
    C ADJUST COEFFICIENTS FOR ORIGINAL RANGE
    C OF X
    DO 80 J=1,L
    C(J) = C(J) * C1
    C1 = (XMAX + YMIN) / 2.0
    DO 90 I=1,L
    W(I)=1.0
    DO 90 J=1,L
    C(J) = -C1 * C(J-1) + C(J)
    C INITIATE PRINT OF ERROR ANALYSIS IF LIST .NE. 0
    C IF (LIST.FO.1) PRINT 1001
    C COMPUTE MAXIMUM AND ROOT MEAN SQUARE ERRORS
    C AND OUTPUT PROC ANALYSIS IF LIST .NE. 0
    EMAX=0.0
    SUM=C.0
    DO 120 I=1,M
    VC=C(I)
    DO 100 J=1,K
    VC=VC*(1+C(J+1))
    CIP=VC-Y(I)
    IF (LIST.FO.0) GO TO 120
    IF (I .GT. LI) GO TO 110
    PRINT 1002, I, X(I), Y(I), VC, DIF, C(I)
    GO TO 120
    110 PRINT 1002, I, X(I), Y(I), VC, DIF
    120 EMAX=MAX(EMAX,ABS(CIP))
    130 SUM=SUM+DIF**2
    
```

PLS0011  
 PLS0012  
 PLS0013  
 PLS0014  
 PLS0015  
 PLS0016  
 PLS0017  
 PLS0018  
 PLS0019  
 PLS0020  
 PLS0021  
 PLS0022  
 PLS0023  
 PLS0024  
 PLS0025  
 PLS0026  
 PLS0027  
 PLS0028  
 PLS0029  
 PLS0030  
 PLS0031  
 PLS0032  
 PLS0033  
 PLS0034  
 PLS0035  
 PLS0036  
 PLS0037  
 PLS0038  
 PLS0039  
 PLS0040  
 PLS0041  
 PLS0042  
 PLS0043  
 PLS0044  
 PLS0045  
 PLS0046  
 PLS0047  
 PLS0048  
 PLS0049  
 PLS0050  
 PLS0051  
 PLS0052  
 PLS0053  
 PLS0054  
 PLS0055  
 PLS0056  
 PLS0057  
 PLS0058  
 PLS0059  
 PLS0060  
 PLS0061  
 PLS0062  
 PLS0063  
 PLS0064  
 PLS0065

67

```

170 ERMS=PORT(SUM/FLOAT(N))
    IF (LIST.EQ.1) PRINT 1003, EMAX, ERMS, EMEQ
    RETURN
C   GIVE ERROR MESSAGE AND RETURN TO
C   SYSTEM VIA FXFM
C   200 PRINT 1000, N, K
    CALL SYSTEM (200,1L)
    RETURN
1000 FORMAT (3HON=11,2H K=,11,20HINCORRECT FOR SUBROUTINE PLSC)
1001 FORMAT (1M,20X,12MPLSD POLYNOMIAL LEAST SQUARE
    *2MPLSD FIT ERROR ANALYSIS//
    *4M0 1 11X,3M2 - GIVN,11X,4M1 - GIVFM,11X,
1002 GIVCHY - FITTED,12X,5M2COOP,16X,4M3(11//)
1003 FORMAT (1H,9X,5M2EMAX=,10E15.6,9X,5M2ERMS=,E15.6,
    *9X,5M2EMEQ=,E15.4)
    END
PLSC0100
PLSC0101
PLSC0102
PLSC0103
PLSC0104
PLSC0105
PLSC0106
PLSC0107
PLSC0108
PLSC0109
PLSC0110
PLSC0111
PLSC0112
PLSC0113
PLSC0114
PLSC0115
PLSC0116
PLSC0117
PLSC0118
PLSC0119
PLSC0120
PLSC0121
PLSC0122
PLSC0123
PLSC0124
PLSC0125
PLSC0126
PLSC0127
PLSC0128
PLSC0129
PLSC0130

```

```

5      SUBROUTINE SIMPS(A,B,TOL,MIN,MAX,ALARM,JTCL)
      CALLING SEQUENCE
      CALL SIMPS(A,B,TOL,MIN,MAX,ALARM,ALARM,TOL)
      REMBER LIMIT
      TOL=MAX(S,MIN,SIGNIF, DIGITS
      JMAX=MIN NO. OF ITERATIONS ALLOWED
      JMIN=MIN NO. OF ITERATIONS
      ANOM=VALUE OF INTEGRAL
      ALARM=1. INDICATES CONVERGENCE
           =1. CONVERGENCE
      JTCL=NO. OF ITERATIONS REQUIRED FOR CONVERGENCE
      SINCE REQUIRED WAITING OF SUBROUTINE FNEVAL TO EVALUATE INTEGRAND
      FNEVAL(//MIN,MAX,MIN-TOL,MAX+TOL) DID NOT CONVERGE AFTER
      12,75,2X,17 ITERATIONS(//)
      10      GO TO 74
      15      ALARM=1
      20      JTCL=1
      25      CALL FNEVAL(A,B)
      30      CALL FNEVAL(A,B)
      35      CALL FNEVAL(A,B)
      40      CALL FNEVAL(A,B)
      45      CALL FNEVAL(A,B)
      50      CALL FNEVAL(A,B)
      55      CALL FNEVAL(A,B)
      60      CALL FNEVAL(A,B)
      65      CALL FNEVAL(A,B)
      70      CALL FNEVAL(A,B)
      75      CALL FNEVAL(A,B)
      80      CALL FNEVAL(A,B)
      85      CALL FNEVAL(A,B)
      90      CALL FNEVAL(A,B)
      95      CALL FNEVAL(A,B)
      100     CALL FNEVAL(A,B)
      105     CALL FNEVAL(A,B)
      110     CALL FNEVAL(A,B)
      115     CALL FNEVAL(A,B)
      120     CALL FNEVAL(A,B)
      125     CALL FNEVAL(A,B)
      130     CALL FNEVAL(A,B)
      135     CALL FNEVAL(A,B)
      140     CALL FNEVAL(A,B)
      145     CALL FNEVAL(A,B)
      150     CALL FNEVAL(A,B)
      155     CALL FNEVAL(A,B)
      160     CALL FNEVAL(A,B)
      165     CALL FNEVAL(A,B)
      170     CALL FNEVAL(A,B)
      175     CALL FNEVAL(A,B)
      180     CALL FNEVAL(A,B)
      185     CALL FNEVAL(A,B)
      190     CALL FNEVAL(A,B)
      195     CALL FNEVAL(A,B)
      200     CALL FNEVAL(A,B)
      205     CALL FNEVAL(A,B)
      210     CALL FNEVAL(A,B)
      215     CALL FNEVAL(A,B)
      220     CALL FNEVAL(A,B)
      225     CALL FNEVAL(A,B)
      230     CALL FNEVAL(A,B)
      235     CALL FNEVAL(A,B)
      240     CALL FNEVAL(A,B)
      245     CALL FNEVAL(A,B)
      250     CALL FNEVAL(A,B)
      255     CALL FNEVAL(A,B)
      260     CALL FNEVAL(A,B)
      265     CALL FNEVAL(A,B)
      270     CALL FNEVAL(A,B)
      275     CALL FNEVAL(A,B)
      280     CALL FNEVAL(A,B)
      285     CALL FNEVAL(A,B)
      290     CALL FNEVAL(A,B)
      295     CALL FNEVAL(A,B)
      300     CALL FNEVAL(A,B)
      305     CALL FNEVAL(A,B)
      310     CALL FNEVAL(A,B)
      315     CALL FNEVAL(A,B)
      320     CALL FNEVAL(A,B)
      325     CALL FNEVAL(A,B)
      330     CALL FNEVAL(A,B)
      335     CALL FNEVAL(A,B)
      340     CALL FNEVAL(A,B)
      345     CALL FNEVAL(A,B)
      350     CALL FNEVAL(A,B)
      355     CALL FNEVAL(A,B)
      360     CALL FNEVAL(A,B)
      365     CALL FNEVAL(A,B)
      370     CALL FNEVAL(A,B)
      375     CALL FNEVAL(A,B)
      380     CALL FNEVAL(A,B)
      385     CALL FNEVAL(A,B)
      390     CALL FNEVAL(A,B)
      395     CALL FNEVAL(A,B)
      400     CALL FNEVAL(A,B)
      405     CALL FNEVAL(A,B)
      410     CALL FNEVAL(A,B)
      415     CALL FNEVAL(A,B)
      420     CALL FNEVAL(A,B)
      425     CALL FNEVAL(A,B)
      430     CALL FNEVAL(A,B)
      435     CALL FNEVAL(A,B)
      440     CALL FNEVAL(A,B)
      445     CALL FNEVAL(A,B)
      450     CALL FNEVAL(A,B)
      455     CALL FNEVAL(A,B)
      460     CALL FNEVAL(A,B)
      465     CALL FNEVAL(A,B)
      470     CALL FNEVAL(A,B)
      475     CALL FNEVAL(A,B)
      480     CALL FNEVAL(A,B)
      485     CALL FNEVAL(A,B)
      490     CALL FNEVAL(A,B)
      495     CALL FNEVAL(A,B)
      500     CALL FNEVAL(A,B)
      505     CALL FNEVAL(A,B)
      510     CALL FNEVAL(A,B)
      515     CALL FNEVAL(A,B)
      520     CALL FNEVAL(A,B)
      525     CALL FNEVAL(A,B)
      530     CALL FNEVAL(A,B)
      535     CALL FNEVAL(A,B)
      540     CALL FNEVAL(A,B)
      545     CALL FNEVAL(A,B)
      550     CALL FNEVAL(A,B)
      555     CALL FNEVAL(A,B)
      560     CALL FNEVAL(A,B)
      565     CALL FNEVAL(A,B)
      570     CALL FNEVAL(A,B)
      575     CALL FNEVAL(A,B)
      580     CALL FNEVAL(A,B)
      585     CALL FNEVAL(A,B)
      590     CALL FNEVAL(A,B)
      595     CALL FNEVAL(A,B)
      600     CALL FNEVAL(A,B)
      605     CALL FNEVAL(A,B)
      610     CALL FNEVAL(A,B)
      615     CALL FNEVAL(A,B)
      620     CALL FNEVAL(A,B)
      625     CALL FNEVAL(A,B)
      630     CALL FNEVAL(A,B)
      635     CALL FNEVAL(A,B)
      640     CALL FNEVAL(A,B)
      645     CALL FNEVAL(A,B)
      650     CALL FNEVAL(A,B)
      655     CALL FNEVAL(A,B)
      660     CALL FNEVAL(A,B)
      665     CALL FNEVAL(A,B)
      670     CALL FNEVAL(A,B)
      675     CALL FNEVAL(A,B)
      680     CALL FNEVAL(A,B)
      685     CALL FNEVAL(A,B)
      690     CALL FNEVAL(A,B)
      695     CALL FNEVAL(A,B)
      700     CALL FNEVAL(A,B)
      705     CALL FNEVAL(A,B)
      710     CALL FNEVAL(A,B)
      715     CALL FNEVAL(A,B)
      720     CALL FNEVAL(A,B)
      725     CALL FNEVAL(A,B)
      730     CALL FNEVAL(A,B)
      735     CALL FNEVAL(A,B)
      740     CALL FNEVAL(A,B)
      745     CALL FNEVAL(A,B)
      750     CALL FNEVAL(A,B)
      755     CALL FNEVAL(A,B)
      760     CALL FNEVAL(A,B)
      765     CALL FNEVAL(A,B)
      770     CALL FNEVAL(A,B)
      775     CALL FNEVAL(A,B)
      780     CALL FNEVAL(A,B)
      785     CALL FNEVAL(A,B)
      790     CALL FNEVAL(A,B)
      795     CALL FNEVAL(A,B)
      800     CALL FNEVAL(A,B)
      805     CALL FNEVAL(A,B)
      810     CALL FNEVAL(A,B)
      815     CALL FNEVAL(A,B)
      820     CALL FNEVAL(A,B)
      825     CALL FNEVAL(A,B)
      830     CALL FNEVAL(A,B)
      835     CALL FNEVAL(A,B)
      840     CALL FNEVAL(A,B)
      845     CALL FNEVAL(A,B)
      850     CALL FNEVAL(A,B)
      855     CALL FNEVAL(A,B)
      860     CALL FNEVAL(A,B)
      865     CALL FNEVAL(A,B)
      870     CALL FNEVAL(A,B)
      875     CALL FNEVAL(A,B)
      880     CALL FNEVAL(A,B)
      885     CALL FNEVAL(A,B)
      890     CALL FNEVAL(A,B)
      895     CALL FNEVAL(A,B)
      900     CALL FNEVAL(A,B)
      905     CALL FNEVAL(A,B)
      910     CALL FNEVAL(A,B)
      915     CALL FNEVAL(A,B)
      920     CALL FNEVAL(A,B)
      925     CALL FNEVAL(A,B)
      930     CALL FNEVAL(A,B)
      935     CALL FNEVAL(A,B)
      940     CALL FNEVAL(A,B)
      945     CALL FNEVAL(A,B)
      950     CALL FNEVAL(A,B)
      955     CALL FNEVAL(A,B)
      960     CALL FNEVAL(A,B)
      965     CALL FNEVAL(A,B)
      970     CALL FNEVAL(A,B)
      975     CALL FNEVAL(A,B)
      980     CALL FNEVAL(A,B)
      985     CALL FNEVAL(A,B)
      990     CALL FNEVAL(A,B)
      995     CALL FNEVAL(A,B)
      END

```

Reproduced from best available copy.

69-

AVEPIL TS NACH 1960  
 74 POINTS ARE GIVEN  
 THEY ARE

BY	V	V
1	15100	15100
2	15000	15000
3	14900	14900
4	14800	14800
5	14700	14700
6	14600	14600
7	14500	14500
8	14400	14400
9	14300	14300
10	14200	14200
11	14100	14100
12	14000	14000
13	13900	13900
14	13800	13800
15	13700	13700
16	13600	13600
17	13500	13500
18	13400	13400
19	13300	13300
20	13200	13200
21	13100	13100
22	13000	13000
23	12900	12900
24	12800	12800
25	12700	12700
26	12600	12600
27	12500	12500
28	12400	12400
29	12300	12300
30	12200	12200
31	12100	12100
32	12000	12000
33	11900	11900
34	11800	11800

POINT 25 IS OFFERED IN FULL TO BE EQUAL TO POINT 1 FOR CLOSURE.  
 AIRPORTS OPERATING UNDER THE AIRPORTS ACT OF 1946.  
 DENSITY 2000-2000 MICROFILMS 2000-2000 MICROFILMS 2000-2000  
 REYNOLDS NUMBERS 2000-2000 MICROFILMS 2000-2000 MICROFILMS

MI	X	Y	PX	PY	YY	CMSCA	SNO	PSI	XXX	YYV	TMETA	VTY
1	589560	3	270500	5	110500	451500	250000	320000	266900	437700	166400	0
2	591700	3	272500	5	112500	453500	251000	320000	266900	437700	166400	0
3	593800	3	274500	5	114500	455500	252000	320000	266900	437700	166400	0
4	595900	3	276500	5	116500	457500	253000	320000	266900	437700	166400	0
5	598000	3	278500	5	118500	459500	254000	320000	266900	437700	166400	0
6	600100	3	280500	5	120500	461500	255000	320000	266900	437700	166400	0
7	602200	3	282500	5	122500	463500	256000	320000	266900	437700	166400	0
8	604300	3	284500	5	124500	465500	257000	320000	266900	437700	166400	0
9	606400	3	286500	5	126500	467500	258000	320000	266900	437700	166400	0
10	608500	3	288500	5	128500	469500	259000	320000	266900	437700	166400	0
11	610600	3	290500	5	130500	471500	260000	320000	266900	437700	166400	0
12	612700	3	292500	5	132500	473500	261000	320000	266900	437700	166400	0
13	614800	3	294500	5	134500	475500	262000	320000	266900	437700	166400	0
14	616900	3	296500	5	136500	477500	263000	320000	266900	437700	166400	0
15	619000	3	298500	5	138500	479500	264000	320000	266900	437700	166400	0
16	621100	3	300500	5	140500	481500	265000	320000	266900	437700	166400	0
17	623200	3	302500	5	142500	483500	266000	320000	266900	437700	166400	0
18	625300	3	304500	5	144500	485500	267000	320000	266900	437700	166400	0
19	627400	3	306500	5	146500	487500	268000	320000	266900	437700	166400	0
20	629500	3	308500	5	148500	489500	269000	320000	266900	437700	166400	0
21	631600	3	310500	5	150500	491500	270000	320000	266900	437700	166400	0
22	633700	3	312500	5	152500	493500	271000	320000	266900	437700	166400	0
23	635800	3	314500	5	154500	495500	272000	320000	266900	437700	166400	0
24	637900	3	316500	5	156500	497500	273000	320000	266900	437700	166400	0
25	640000	3	318500	5	158500	499500	274000	320000	266900	437700	166400	0
26	642100	3	320500	5	160500	501500	275000	320000	266900	437700	166400	0
27	644200	3	322500	5	162500	503500	276000	320000	266900	437700	166400	0
28	646300	3	324500	5	164500	505500	277000	320000	266900	437700	166400	0
29	648400	3	326500	5	166500	507500	278000	320000	266900	437700	166400	0
30	650500	3	328500	5	168500	509500	279000	320000	266900	437700	166400	0
31	652600	3	330500	5	170500	511500	280000	320000	266900	437700	166400	0
32	654700	3	332500	5	172500	513500	281000	320000	266900	437700	166400	0
33	656800	3	334500	5	174500	515500	282000	320000	266900	437700	166400	0
34	658900	3	336500	5	176500	517500	283000	320000	266900	437700	166400	0
35	661000	3	338500	5	178500	519500	284000	320000	266900	437700	166400	0
36	663100	3	340500	5	180500	521500	285000	320000	266900	437700	166400	0
37	665200	3	342500	5	182500	523500	286000	320000	266900	437700	166400	0
38	667300	3	344500	5	184500	525500	287000	320000	266900	437700	166400	0
39	669400	3	346500	5	186500	527500	288000	320000	266900	437700	166400	0
40	671500	3	348500	5	188500	529500	289000	320000	266900	437700	166400	0
41	673600	3	350500	5	190500	531500	290000	320000	266900	437700	166400	0
42	675700	3	352500	5	192500	533500	291000	320000	266900	437700	166400	0
43	677800	3	354500	5	194500	535500	292000	320000	266900	437700	166400	0
44	679900	3	356500	5	196500	537500	293000	320000	266900	437700	166400	0
45	682000	3	358500	5	198500	539500	294000	320000	266900	437700	166400	0
46	684100	3	360500	5	200500	541500	295000	320000	266900	437700	166400	0
47	686200	3	362500	5	202500	543500	296000	320000	266900	437700	166400	0
48	688300	3	364500	5	204500	545500	297000	320000	266900	437700	166400	0
49	690400	3	366500	5	206500	547500	298000	320000	266900	437700	166400	0
50	692500	3	368500	5	208500	549500	299000	320000	266900	437700	166400	0
51	694600	3	370500	5	210500	551500	300000	320000	266900	437700	166400	0
52	696700	3	372500	5	212500	553500	301000	320000	266900	437700	166400	0
53	698800	3	374500	5	214500	555500	302000	320000	266900	437700	166400	0
54	700900	3	376500	5	216500	557500	303000	320000	266900	437700	166400	0
55	703000	3	378500	5	218500	559500	304000	320000	266900	437700	166400	0
56	705100	3	380500	5	220500	561500	305000	320000	266900	437700	166400	0
57	707200	3	382500	5	222500	563500	306000	320000	266900	437700	166400	0
58	709300	3	384500	5	224500	565500	307000	320000	266900	437700	166400	0
59	711400	3	386500	5	226500	567500	308000	320000	266900	437700	166400	0
60	713500	3	388500	5	228500	569500	309000	320000	266900	437700	166400	0
61	715600	3	390500	5	230500	571500	310000	320000	266900	437700	166400	0

Reproduced from  
best available copy.

Reproduced from  
best available copy.

24 --201140V --2140C-78  
25 --1769E+00 --.416E-01  
26 --1554E+00 --.3576E-01  
27 --1132E+00 --.766E-02  
28 --1102E+00 --.3649E-01  
29 --7749E-01 --.3647E-01  
30 --4650E-01 --.7747E-01  
31 --2795E-01 --.2076E-01  
32 --4476E-02 --.2641E-01  
33 --5971E-01 --.1677E-01  
34 --9192E-01 --.9769E-02  
35 --1009E+01 --.1654E-01

C  
--2205E-03 --.2176E-07  
--3550E-02 --.3274E-07  
--1856E-01 --.1571E-01  
--2270E-01 --.1687E-01  
--5584E-01 --.5839E-01  
--5555E-01 --.7681E-01

PMIS .6970E+11 EX .2100E+00 ALGMAE 1.0 nrc betaE .0554E+00 nrc  
CIRCULATION .5264E+01 LIFE .3177E+01







UPRR SURPAGE  
 1 1000000  
 2 1000000  
 3 1000000  
 4 1000000  
 5 1000000  
 6 1000000  
 7 1000000  
 8 1000000  
 9 1000000  
 10 1000000  
 11 1000000  
 12 1000000  
 13 1000000  
 14 1000000  
 15 1000000  
 16 1000000  
 17 1000000  
 18 1000000  
 19 1000000  
 20 1000000  
 21 1000000  
 22 1000000  
 23 1000000  
 24 1000000  
 25 1000000  
 26 1000000  
 27 1000000  
 28 1000000  
 29 1000000  
 30 1000000  
 31 1000000  
 32 1000000  
 33 1000000  
 34 1000000  
 35 1000000  
 36 1000000  
 37 1000000  
 38 1000000  
 39 1000000  
 40 1000000  
 41 1000000  
 42 1000000  
 43 1000000  
 44 1000000  
 45 1000000  
 46 1000000  
 47 1000000  
 48 1000000  
 49 1000000  
 50 1000000  
 51 1000000  
 52 1000000  
 53 1000000  
 54 1000000  
 55 1000000  
 56 1000000  
 57 1000000  
 58 1000000  
 59 1000000  
 60 1000000  
 61 1000000  
 62 1000000  
 63 1000000  
 64 1000000  
 65 1000000  
 66 1000000  
 67 1000000  
 68 1000000  
 69 1000000  
 70 1000000  
 71 1000000  
 72 1000000  
 73 1000000  
 74 1000000  
 75 1000000  
 76 1000000  
 77 1000000  
 78 1000000  
 79 1000000  
 80 1000000  
 81 1000000  
 82 1000000  
 83 1000000  
 84 1000000  
 85 1000000  
 86 1000000  
 87 1000000  
 88 1000000  
 89 1000000  
 90 1000000  
 91 1000000  
 92 1000000  
 93 1000000  
 94 1000000  
 95 1000000  
 96 1000000  
 97 1000000  
 98 1000000  
 99 1000000  
 100 1000000

UPRR SURPAGE  
 1 1000000  
 2 1000000  
 3 1000000  
 4 1000000  
 5 1000000  
 6 1000000  
 7 1000000  
 8 1000000  
 9 1000000  
 10 1000000  
 11 1000000  
 12 1000000  
 13 1000000  
 14 1000000  
 15 1000000  
 16 1000000  
 17 1000000  
 18 1000000  
 19 1000000  
 20 1000000  
 21 1000000  
 22 1000000  
 23 1000000  
 24 1000000  
 25 1000000  
 26 1000000  
 27 1000000  
 28 1000000  
 29 1000000  
 30 1000000  
 31 1000000  
 32 1000000  
 33 1000000  
 34 1000000  
 35 1000000  
 36 1000000  
 37 1000000  
 38 1000000  
 39 1000000  
 40 1000000  
 41 1000000  
 42 1000000  
 43 1000000  
 44 1000000  
 45 1000000  
 46 1000000  
 47 1000000  
 48 1000000  
 49 1000000  
 50 1000000  
 51 1000000  
 52 1000000  
 53 1000000  
 54 1000000  
 55 1000000  
 56 1000000  
 57 1000000  
 58 1000000  
 59 1000000  
 60 1000000  
 61 1000000  
 62 1000000  
 63 1000000  
 64 1000000  
 65 1000000  
 66 1000000  
 67 1000000  
 68 1000000  
 69 1000000  
 70 1000000  
 71 1000000  
 72 1000000  
 73 1000000  
 74 1000000  
 75 1000000  
 76 1000000  
 77 1000000  
 78 1000000  
 79 1000000  
 80 1000000  
 81 1000000  
 82 1000000  
 83 1000000  
 84 1000000  
 85 1000000  
 86 1000000  
 87 1000000  
 88 1000000  
 89 1000000  
 90 1000000  
 91 1000000  
 92 1000000  
 93 1000000  
 94 1000000  
 95 1000000  
 96 1000000  
 97 1000000  
 98 1000000  
 99 1000000  
 100 1000000

STATION IS COMPLETE.

Vita

Ellie B. Underwood, Jr., was born on 27 January 1939 in Beeville, Texas. He was graduated in June 1956 from Ballinger High School, Ballinger, Texas. In June 1961, he was awarded a Bachelor of Science degree in Aerospace Engineering from the University of Texas, Austin, Texas, and was commissioned in the United States Air Force at the same time. In June 1960, he was assigned to the Air Force Institute of Technology, Wright-Patterson Air Force Base, Ohio.

Permanent Address: P.O. Box 592  
Ballinger, Texas 76821

This thesis was typed by Jane Manemann.